LMSC-HEC TR F225961

Duct Flow Nonuniformities – Effect of Struts in SSME HGM II+ – Final Report

22 June 1988

Contract NAS8-37359

Prepared for

NATIONAL AERONAUTICS AND SPACE ADMINISTRATION
MARSHALL SPACE FLIGHT CENTER, AL 35812

By

Roger Burke

Lockheed
Missiles & Space Company, Inc.
Huntsville Engineering Center
4800 Bradford Blvd., Huntsville, AL 35807

FOREWORD

This final report documents numerical results obtained by personnel of the Computational Mechanics Section at Lockheed's Huntsville Engineering Center under Contract NAS8-37359, "Duct Flow Nonuniformities Study."

The NASA-MSFC Contracting Officer's Representative for this study is Dr. Paul K. McConnaughey, ED32.

CONTENTS

LIST OF FIGURES

LOCKHEED–HUNTSVILLE ENGINEERING CENTER

CONTENTS (Concluded)

1. INTRODUCTION

This study consists of an analysis of flow through the Space Shuttle Main
Engine (SSME) Hot Gas Manifold (HGM) for the purpose of understanding and
quantifying the flow environment and, in particular, the flow through a region
of structural supports located between the inner and outer walls of the HGM.
The primary task of the study, as defined by NASA-MSFC, is to assess and
develop the computational capability for analyzing detailed three-dimensional
flow through the HGM support strut region to be incorporated into a full fuel-
side HGM analysis. Secondarily, computed results are to be compared with
available experimental results.

Figure 1 shows the SSME powerhead configuration. The turbine is run by a
hot gas, produced in the preburner by burning the fuel at high pressure and
high temperature. Having performed work on the turbine, this gas enters an
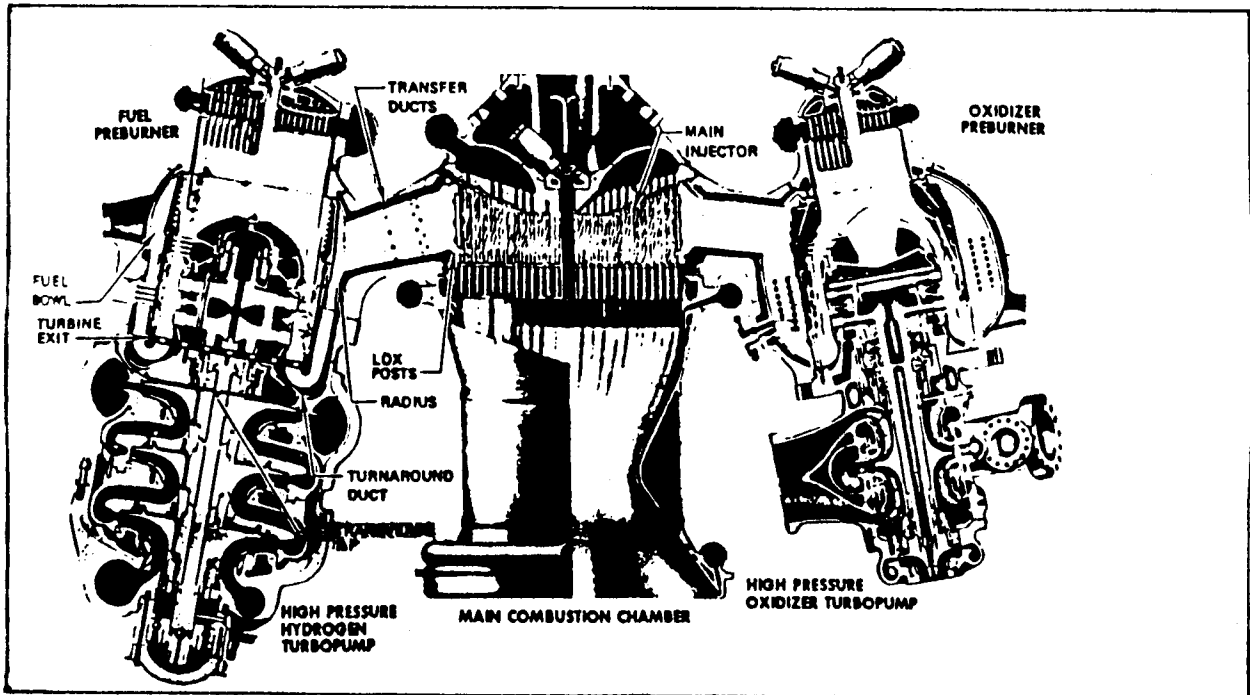
Fig. 1 SSME Powerhead Configuration

1

annular turnaround duct (TAD), which changes the direction of the mean flow by 180 deg. The gas then passes through an assembly of struts and posts before diffusing into a fuel bowl. The gas flows from the fuel bowl into the main injector through several transfer ducts. The high gas temperature causes the flow to be practically incompressible, with a Mach number of less than 0.12.

A more detailed picture of the strut-post assembly is seen in Fig. 2a, which presents an idealized cross-sectional view of the TAD, with the flow direction normal to the plane of the paper. Figure 2b shows a different perspective, with the flow direction in the plane of the paper.

As a first step toward simulating the three-dimensional viscous, turbulent flow in the HGM strut region, two simplified test geometries were investigated, consisting of two-dimensional flow around a strut, and three-dimensional flow around a strut in an annulus. Both laminar and turbulent calculations were performed. A multiple-zone procedure was implemented to calculate two-dimensional laminar flow around two struts placed in parallel, with each strut confined to a separate computational zone. Turbulent, multiple-zone calculations were then performed for the flow around a strut inside an annular turnaround duct. In order to study the applicability of the proposed methodology to wing-body configurations, calculations were also performed for external flow around a wing mounted on a flat plate, and the results compared against wind tunnel data. Details of the approach used to numerically simulate these flow fields are contained in Section 2. Computational results are presented and discussed in Section 3, and concluding remarks are outlined in Section 4.
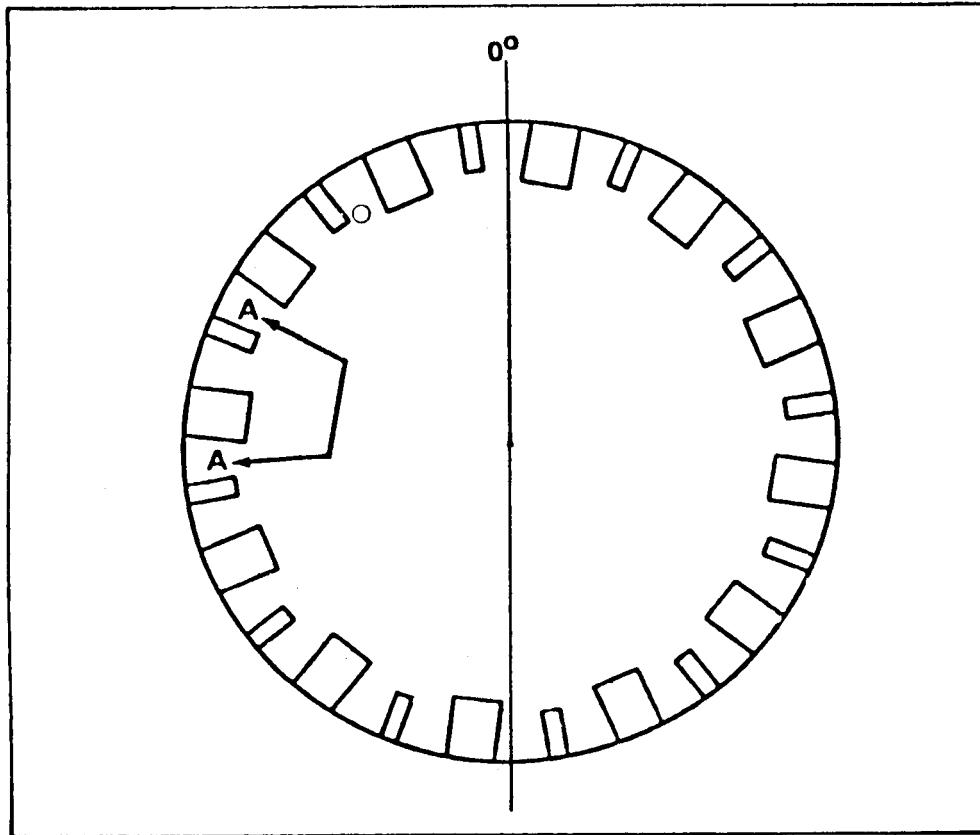
a. Idealized Top View of TAD Strut and Post Assembly
(Flow direction is normal to plane of paper.)
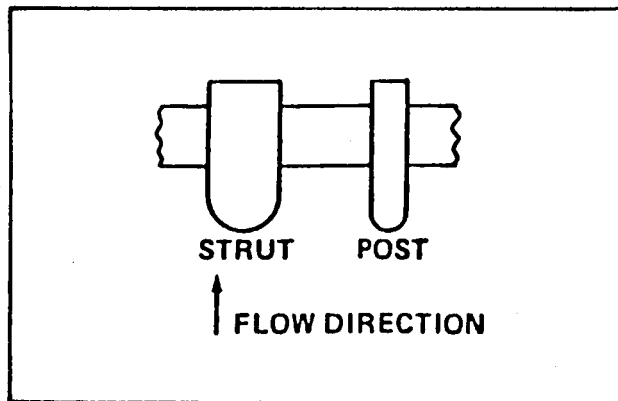
b. View A, with Flow Direction in Plane of Paper

Fig. 2 Strut and Post Assembly

3

2. APPROACH

2.1 GENERAL DESCRIPTION

Computations were performed using the INS3D code for incompressible three-dimensional flow which was developed by Kwak et al. (Ref. 1). The code solves the full three-dimensional incompressible Navier-Stokes equations, using a pseudo-compressibility approach to handle the pressure. Reference 1 provides a detailed description of the INS3D methodology.

2.2 MULTIPLE-ZONE METHOD

The calculations in this study were performed on the NASA-Ames Cray X-MP 4/8, which has a maximum allowable CPU memory of approximately four million words. A full three-dimensional, viscous simulation of the flow in the HGM strut region will require more computational mesh points than can be handled by this size of storage, thus necessitating the use of a multiple-zone method. In this method, the solution is obtained by dividing the computational domain of interest into several zones, generating the grid for each zone separately, then solving the equations of motion in each zone to update the interior points. The points at the interface between zones are updated using a zonal boundary treatment which ensures smooth continuation of the solution between zones. Various zonal boundary strategies have been proposed (Ref. 2 and 3). The approach used in this study consists of a simple double-plane overlapping, as described by Chang et al. (Ref. 4) and Holst et al. (Ref. 5).

As an illustration of the zonal boundary treatment scheme, Fig. 3 shows a double-plane overlapping of two zones; the grid points of zone 1 are designated by circles, while those of zone 2 are marked by diamonds. The last two grid lines of zone 1 (j-1 and j) are seen to overlap with the first two lines

4
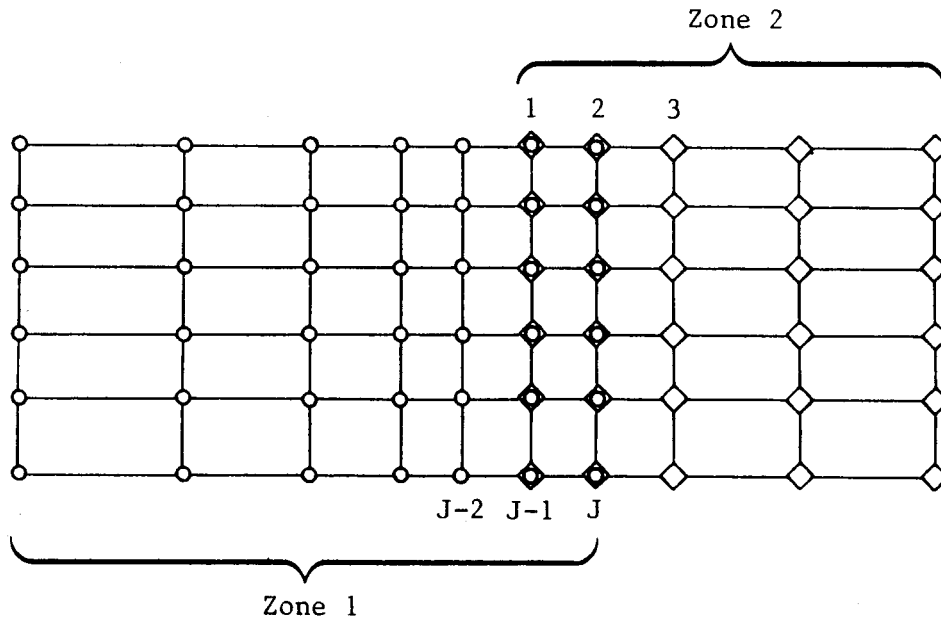
Fig. 3 Zonal Boundary Treatment Scheme

AR-88-022
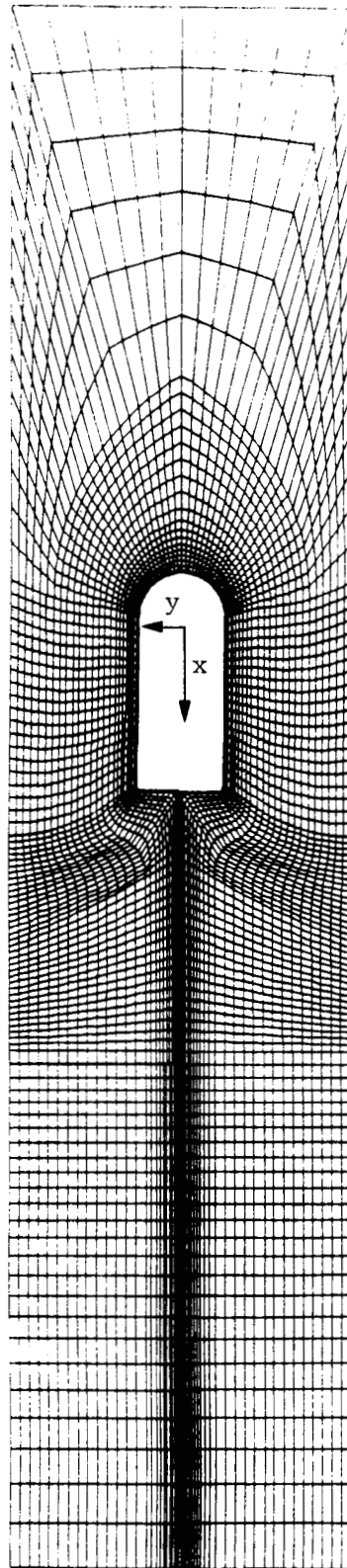
Fig. 4 Mesh System Around Two-Dimensional Strut

LOCKHEED–HUNTSVILLE ENGINEERING CENTER

of zone 2. Upon updating the interior nodes of zone 1 using the INS3D integration scheme, the values of the variables at the first line of zone 2 are set equal to the updated values of line j-1 in zone 1. Next, the interior points of zone 2 are computed, and the newly calculated values on line 2 in zone 2 are used to update line J in zone 1. This procedure assumes that a one-to-one correspondence exists between the nodes in each zone, which will be the case for the calculations discussed here. In situations where a coarse grid overlaps with a finer grid, an interpolation process is required to carry the information from one grid to another (Refs. 4 and 5). Such an interpolation routine would likely be necessary to multiblock the computational zones containing the struts with the relatively lower density grid of the fuel bowl and transfer ducts.

2.3 GRID

The grids used in the calculations were generated using the Lockheed algebraic grid generation code. The two-dimensional strut and the strut in the annulus has a 3:1 length-to-width ratio, with the distance between struts being four strut widths. The strut in the turnaround duct has a 3.5:1 length-to-width ratio, with the distance between struts being six strut widths. These dimensions coincide with those of the strut assembly in the HGM.

Figure 4 shows the C-type mesh system around the two-dimensional strut. The x-y Cartesian coordinate system is oriented so that x is in the streamwise direction. There are 201 grid lines wrapped around the strut with 26 grid lines extending away from the strut. The grid used in the two-dimensional multiple-zone calculations is presented in Fig. 5. The two zones are seen to overlap one another by a double line of nodes. Computations are first performed on grid 1, and then on grid 2, with the zonal interface being treated as discussed in Section 2.2.

Fig. 5 Grid Used in Two-Dimensional Multiple-Zone Calculations

LOCKHEED–HUNTSVILLE ENGINEERING CENTER

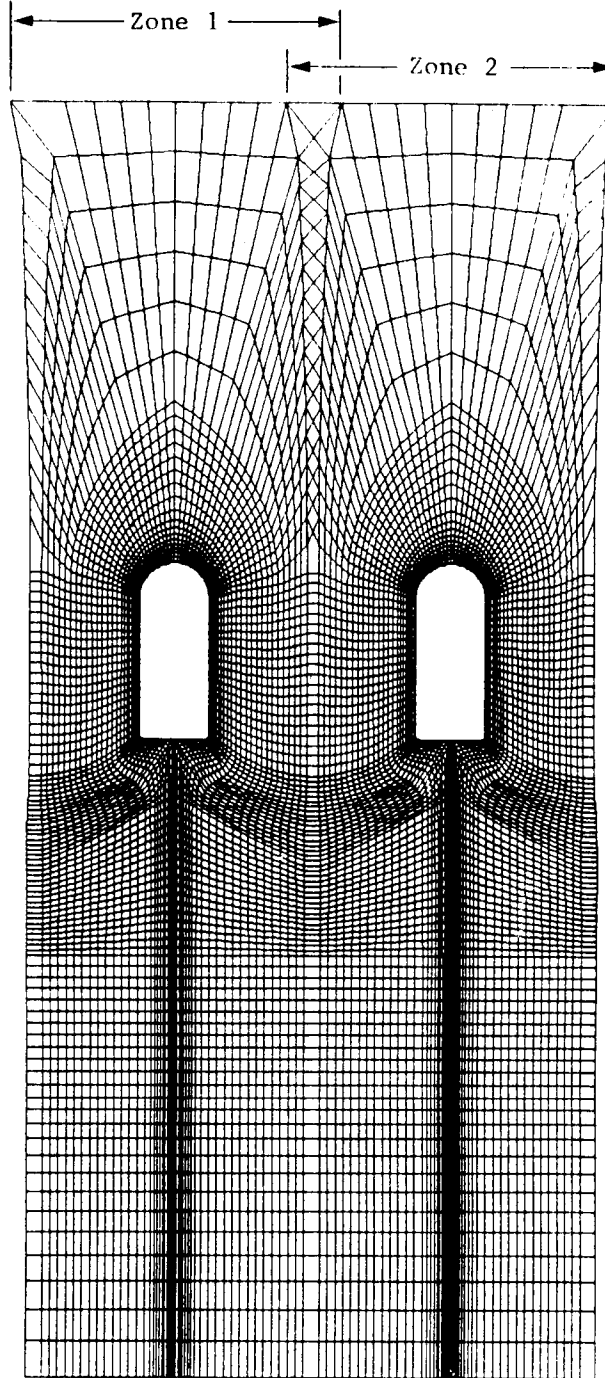The three-dimensional strut in an annulus grid contains 31 planes in the vertical (z) direction. In each annular plane the grid has the same configuration as the two-dimensional grid, resulting in a total of 162006 grid points for the three-dimensional geometry. Figure 6a shows that portion of the grid in the vicinity of the strut indicating all no-slip surfaces in the geometry.

The strut in a turnaround duct grid consists of two zones, shown together in Fig. 6b. Zone 1 encompasses the turnaround duct and has 66 nodes in the streamwise direction, 23 in the lateral direction, and 31 nodes from the inner to outer turnaround duct walls. Zone 2 includes the strut and has a C-type configuration with 197 grid lines wrapped around the strut and 27 grid lines extending away from the strut. In conformity with Zone 1, there are 31 nodes in the vertical direction. The fuel bowl is simulated by a streamwise variation in cross-sectional area aft of the strut. The interface between the two zones is located approximately one strut length ahead of the leading edge of the strut.

The mesh system for the wing on a flat plate configuration consists of a C grid, as shown in Fig. 6c. The grid consists of 95x41x41 points, where I is the coordinate direction along the wing, J is the coordinate direction away from the wing, and K is away from the flat plate.

2.4 BOUNDARY CONDITIONS

Explicit boundary conditions are used in the calculations. No-slip conditions are applied on the solid surfaces. The pressure on these surfaces is determined by requiring that the normal pressure gradient be zero, i.e.,

$$\frac{\partial p}{\partial \hat{\eta}} = 0 \qquad (1)$$

where $\hat{n}$ represents the direction normal to a wall.

Conditions for the downstream boundary are the most difficult to provide, and they require careful specification to avoid numerical instabilities and non-convergence. The downstream values of pressure and velocity are updated
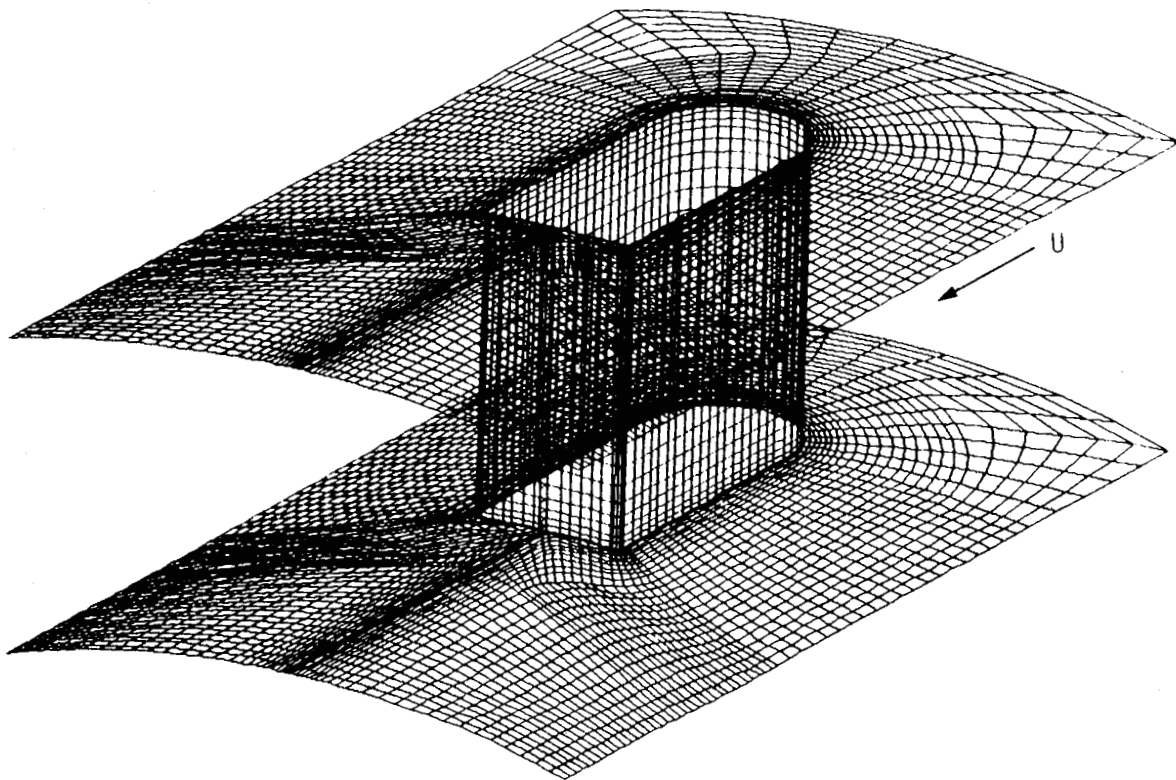
9

Fig. 6a   Strut with Upper and Lower Annulus Surfaces

Fig. 6b   Mesh System for Strut in Turnaround Duct

LOCKHEED–HUNTSVILLE ENGINEERING CENTER
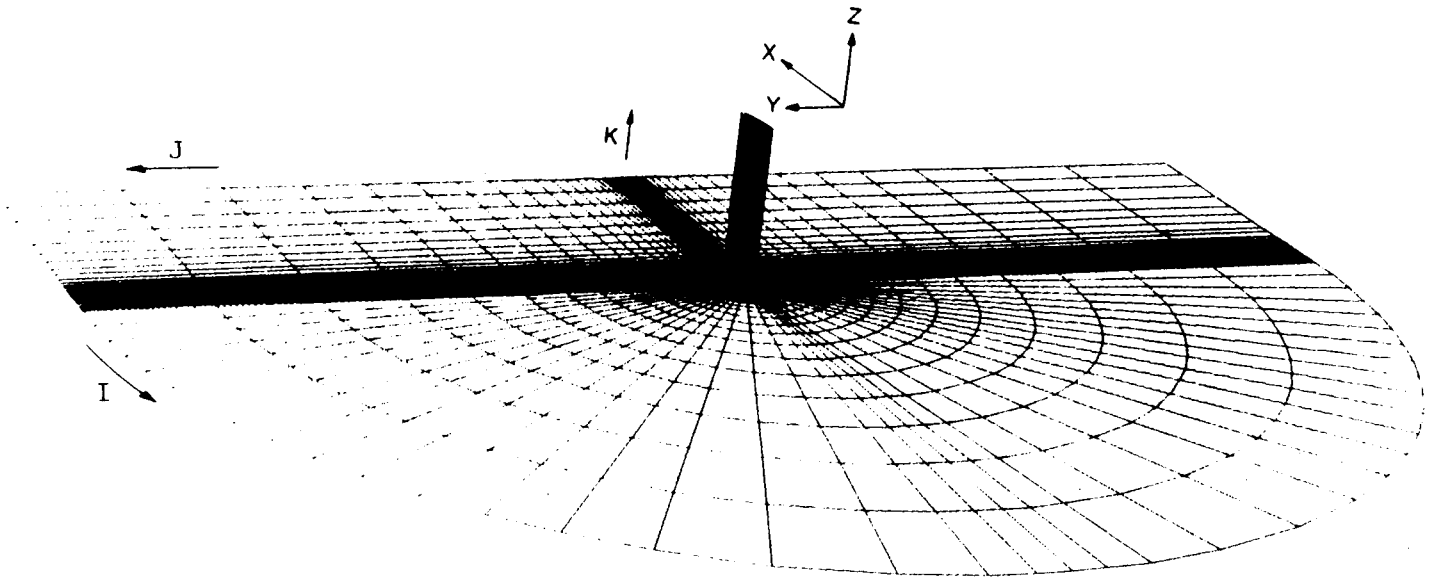
ORIGINAL PAGE IS
OF POOR QUALITY

Fig. 6c   Mesh System for Wing on Flat Plate

in the manner prescribed by Chang et al. (Ref. 4). In this approach, a second-order upwind extrapolation is first used to update the velocities normal to the exit plane. Next, these updated velocities are mass-weighted to conserve the inlet mass flux. A new pressure corresponding to these mass-weighted velocities is then determined to ensure conservation of momentum flux at the outflow.

Periodic boundary conditions are applied at the lateral boundaries to simulate the effect of a row of struts, such as exists in the HGM. The posts, which are located midway between successive struts (Fig. 2b) are treated as no-slip boundary nodes. To date, the posts have been included in two-dimensional laminar calculations only. For the two-dimensional computations uniform static pressure and velocity is assumed known and held fixed at the inlet. For the three-dimensional calculations a uniform static pressure is held fixed at the inlet. The velocity profile at the inlet is also held constant, with the velocity magnitudes being derived from a power law formulation in the vicinity of the inner and outer no-slip surfaces.

For the wing-flat plate case the outer boundary of $J = J_{max}$ (see Fig. 6c) is assumed far enough away so as not to be affected by the interaction region of the wing and flat plate. Accordingly, a static pressure and boundary layer profile are prescribed and held fixed along the outer boundary. Symmetry boundary conditions are applied at $z/c = 2.0$, which corresponds to the mid-height of the wind tunnel used in the experiments.

2.5 TURBULENCE MODEL

Turbulence modeling for complicated internal flows such as a strut between two walls is complicated and not well understood. As such, it was decided, as a first step, to parameterize the turbulent shear stresses using a simple zero equation approach. Specifically, two different algebraic turbulence models were investigated. The Baldwin-Lomax model (Ref. 6) was applied to two-dimensional calculations of flow around a strut. The Baldwin-Lomax model was then modified, as described below, to be able to handle the presence of multiple length scales such as exist in internal flow around a strut between

13

two walls. This modified Baldwin-Lomax model was applied to both the strut inside an annulus, and the strut inside a turnaround duct configurations. A second turbulence model, consisting of a simple mixing length approach, was also investigated for the strut inside a turnaround duct case, and external flow around a wing mounted on a flat plate.

2.5.1 Baldwin-Lomax Model

A Baldwin-Lomax turbulence model (Ref. 6) was used to parameterize the turbulent shear stresses for the two-dimensional flow around a strut. In this approach, an eddy viscosity (μ_t) is calculated for an inner and an outer region. The eddy viscosity for the inner region is based on the Prandtl-Van Driest formulation

$$(\mu_t)_{inner} = \rho \ell^2 |\omega| \tag{2}$$

where

$$\ell = ky \left[1.0 - \exp(-y^+/A^+)\right] \; , \; y^+ = \rho \sqrt{\tau_\omega} \, y/\mu \tag{3}$$

and τ_ω is the wall shear stress. The magnitude of the vorticity $|\omega|$ is given by

$$|\omega| = \left[\left(\frac{\partial u}{\partial y} - \frac{\partial v}{\partial x}\right)^2 + \left(\frac{\partial v}{\partial z} - \frac{\partial w}{\partial y}\right)^2 + \left(\frac{\partial w}{\partial x} - \frac{\partial u}{\partial x}\right)^2\right]^{1/2} \tag{4}$$

The eddy viscosity for the outer region is given by

$$\left(\mu_t\right)_{outer} = \rho \, KC_{cp} \, F_{wake} \, F_{kleb} \, (y) \tag{5}$$

where F_{wake} is the smaller of $Y_{max} \, F_{max}$ or $C_{wk} \, Y_{max} \, U_d^2 \, F_{max}$.

F_{max} is the maximum value of the expression

$$F(y) = y|\omega| \left[1.0 - \exp(-y^+/A^+)\right] \tag{6}$$

14

in a profile and Y_{max} is y at that point. Also

$$F_{kleb}(y) = \left[1.0+5.5(yC_{kleb}/Y_{max})^6 \right]^{-1} \qquad (7)$$

The quantity U_d is the difference between the maximum and minimum values of velocity in a given profile. The constants are assigned the following values: $A^+ = 26$, $C_{cp} = 1.6$, $C_{kleb} = 0.3$, $C_{wk} = 0.25$, and $K = 0.0168$.

As discussed by Mehta et al. (Ref. 7) the above formulation gives $\mu_t = 0.0$ in the wake region when the wake is symmetric, because the Van Driest damping function, Eq. (2), depends on the vorticity on the centerline of the wake, which has the value of zero. Mehta et al. correct for this error by modifying the length scale equation to give

$$\ell = 0.4y \left[1.0 - \exp \{-(y^+/A^+) - (x^+/A^+)\} \right] \qquad , \qquad (8)$$

with

$$x^+ = \begin{cases} 0.0 \text{ if } x < x_b \\ (x - x_b)/L \quad \text{otherwise} \end{cases} \qquad (9)$$

x_b is the x location of the strut trailing edge, and L is the length of the strut.

In the outer region, the definition of F(y) is replaced by

$$F(y) = y|\omega| \left[1.0-\exp \{ -(y^+/A^+) - (x^+/A^+)\} \right] \qquad (10)$$

The eddy viscosity is determined at every point using Eqs. (2) and (5). The smaller of the two values is then used in the governing equations.

The Baldwin-Lomax model described above for flow around a body was modified to be able to handle channel walls by incorporating the approach of Chang et al. (Ref. 4) for flow in the HGM. In their analysis, which did not include the presence of struts, Chang et al adopted an extended Prandtl-Karman mixing length theory, with the mixing length (ℓ) given as

15

$$\frac{\ell}{\delta} = k^2 \left(1 - e^{-\tilde{z}/k}\right)\left(1 - e^{z^+/A^+}\right), \quad z^+ = \rho\sqrt{\tau_\omega}\, z/\mu \tag{11}$$

where $\tilde{z} = z/\delta$.

δ is some characteristic reference length scale which serves to divide the internal flow region into two zones. Figure 7 shows this approach applied to a two-dimensional channel flow. The terms δ_1 and δ_2 are the reference length scales measured from wall 1 and wall 2, respectively. In zone 1, δ_1 is used in Eq. (11), and z and z^+ are computed based on wall 1. In zone 2, δ_2 is used in Equation 11, and z and z^+ are computed based on wall 2. Various ideas have been proposed for δ, including the centerline of the flow domain, location of maximum velocity, and location of minimum vorticity (δ_ω), which is the length scale proposed by Chang et al. The calculations presented here also use δ_ω as the reference length scale.
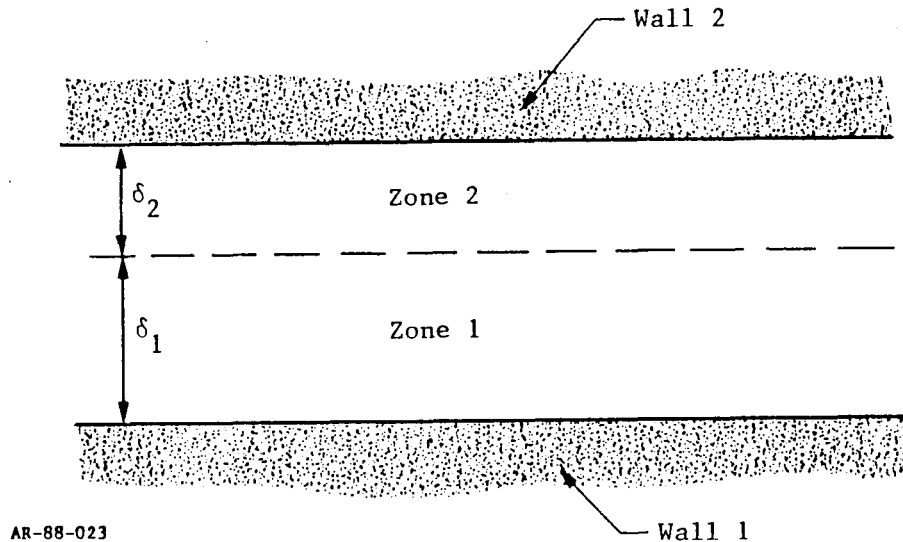

Fig. 7 Mixing Length Regimes for Internal Flow

16

The eddy viscosity in the modified Baldwin-Lomax approach is calculated first by computing μ_t according to Eqs. (2) through (10), which assumes that the strut is the only surface. Next, μ_t is computed using Eq. (11), which assumes that the upper and lower annulus surfaces are the only surfaces, and ignores the presence of the strut. The smaller of the two values of μ_t is then taken as the final value of the eddy viscosity. This idea of calculating two separate eddy viscosities and then taking the smaller of the two values was applied by Gorski et al. (Ref. 8) to the problem of a wing on a single flat plate. It has been extended here to include the case of a strut between two walls.

2.5.2 Mixing Length Model

In addition to the modified Baldwin-Lomax approach described in the previous section, a second algebraic model was investigated in which the turbulent eddy viscosity was given by

$$\mu_t = \rho(k\ell)^2 |\omega|$$

The length scale ℓ is equal to

$$1/\ell = \sum_{i=1}^{3} 1/\ell_i D_i$$

where ℓ_1, ℓ_2, ℓ_3 are the distances from the strut, the lower turnaround duct surface, and the upper turnaround duct surface (R.C. Buggelin, personal communication). Similarly, D_1, D_2, and D_3 are the Van-Driest damping factors associated with each of these surfaces.

Aside from its relative simplicity compared to the modified Baldwin-Lomax model, this approach has the added advantage that the length scale and turbulent eddy viscosity vary smoothly over the flow field. Note that very near the ith surface as

$$1/\ell_i \rightarrow \infty \qquad \mu_t \rightarrow \rho(k\ell_i D_i)^2 |\omega|$$

17

3. RESULTS

This section presents the laminar and turbulent numerical calculations for two-dimensional flow around a strut, three-dimensional internal flow around a strut in an annulus and in a turnaround duct, and external flow around a wing on a flat plate. The results were produced using the graphical display routine PLOT3D, which was developed at NASA-Ames Research Center (Ref. 9).

3.1 TWO-DIMENSIONAL COMPUTATIONS

Two-dimensional laminar and turbulent computations for flow around a strut were performed. The Reynolds number (based on strut width) was 500 for the laminar case and 1.9×10^6 for the turbulent case. The main purpose of these calculations was to work out errors in the boundary and initial condition routines, experiment with the Baldwin-Lomax turbulence model, and develop the capability to perform multiblock calculations, which will be necessary in simulating the flow in the complete three-dimensional HGM strut region.

3.1.1 Laminar

Figures 8 and 9 present velocity and pressure contours for a two-zone laminar calculation of flow around two struts, with each zone representing one strut. Two cases are considered, one without posts between the struts, and one where the posts are included. The angle of incidence in both cases is zero degrees.

As discussed previously, the posts are simulated by treating two lines of nodes on the overlapping nodal planes as no-slip boundary nodes. Velocity vectors in the region of a post treated in this manner are presented in Fig. 10.
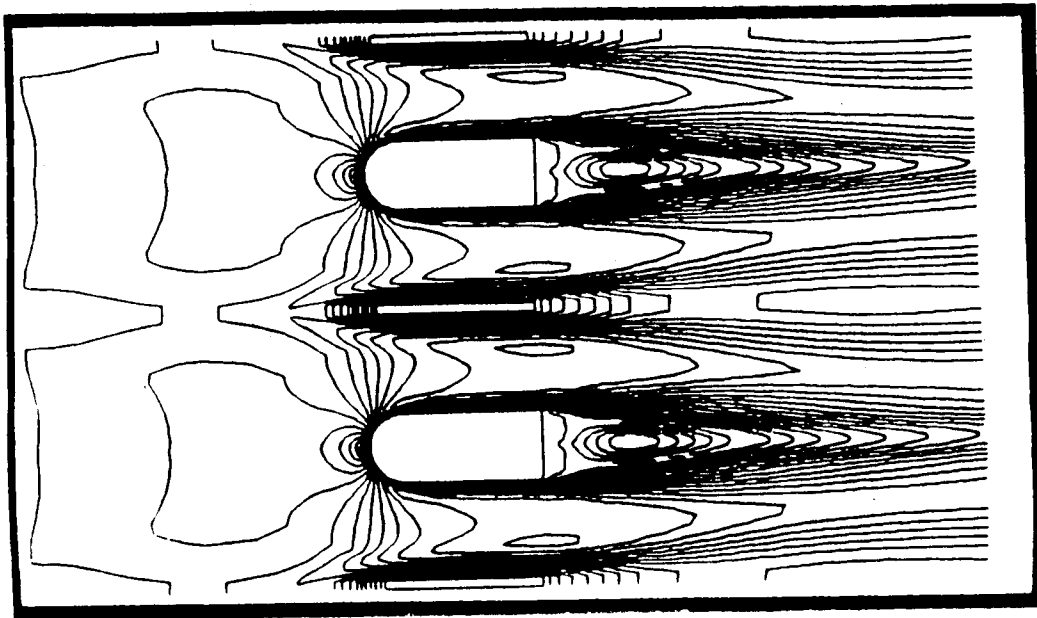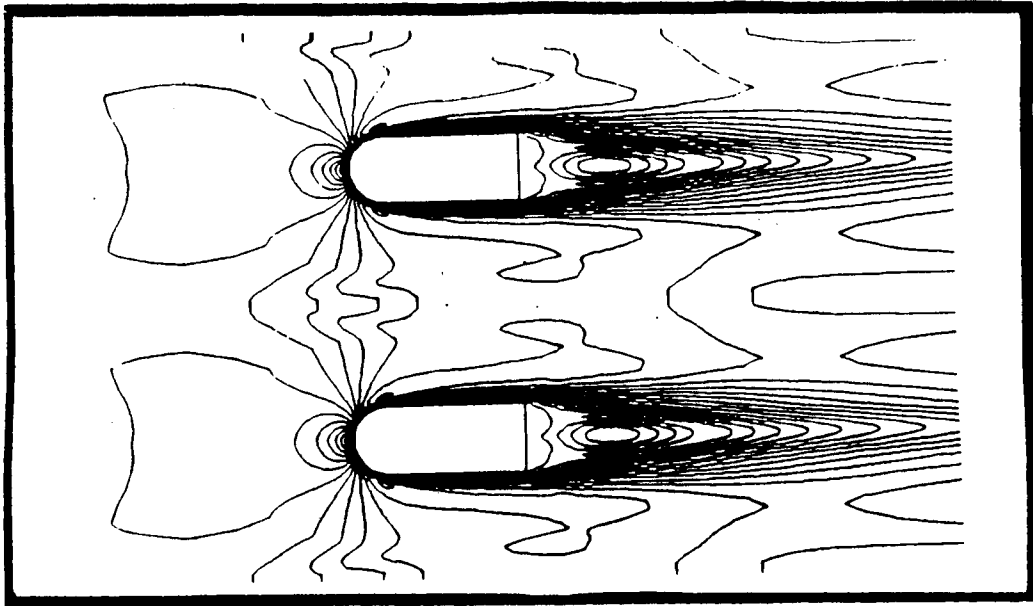
Fig. 8 Velocity Contours for Two Block Two-Dimensional Simulation of Two Struts with (Bottom) and Without Posts
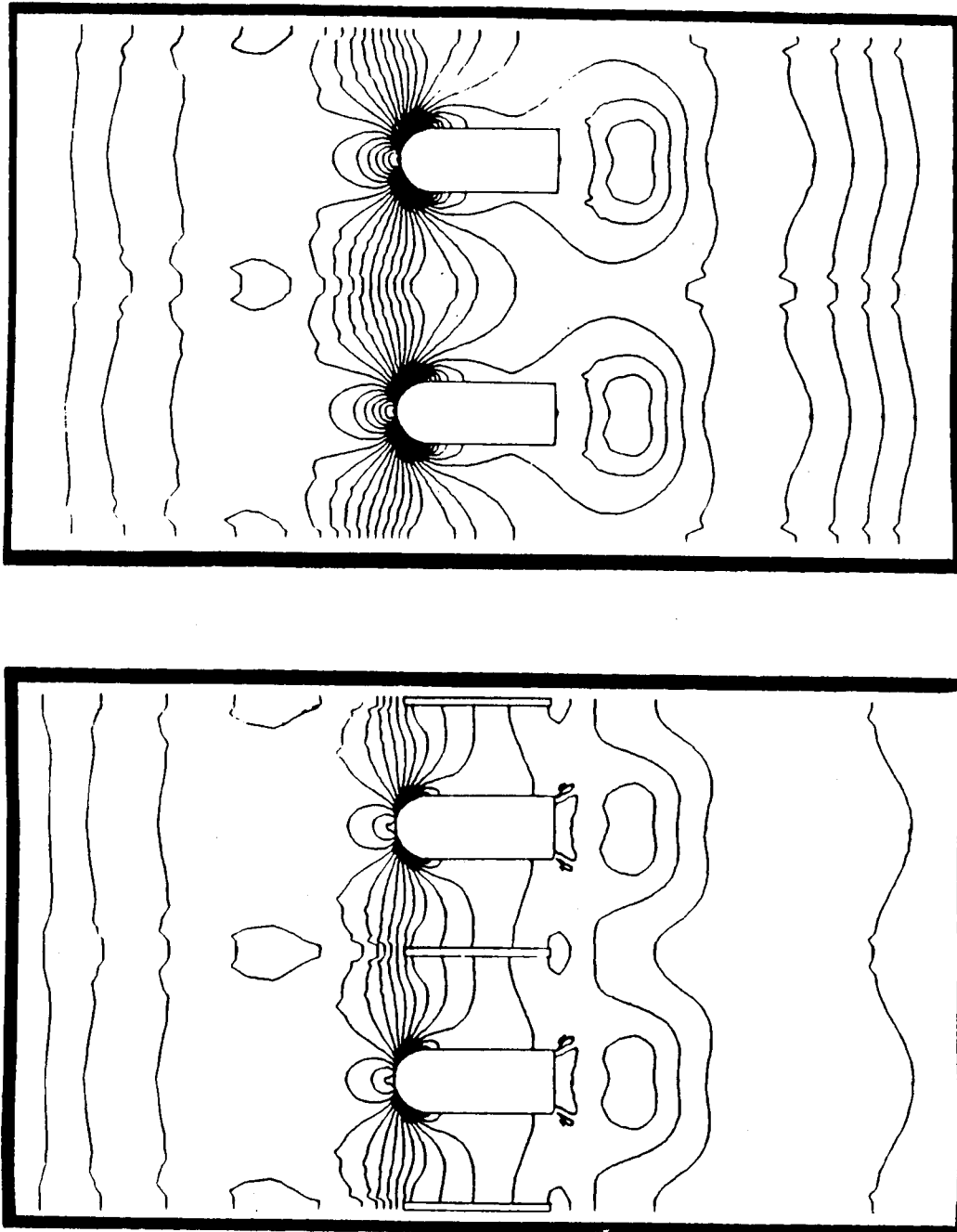
19

Fig. 9   Static Pressure Contours for Two Block Two-Dimensional Simulation
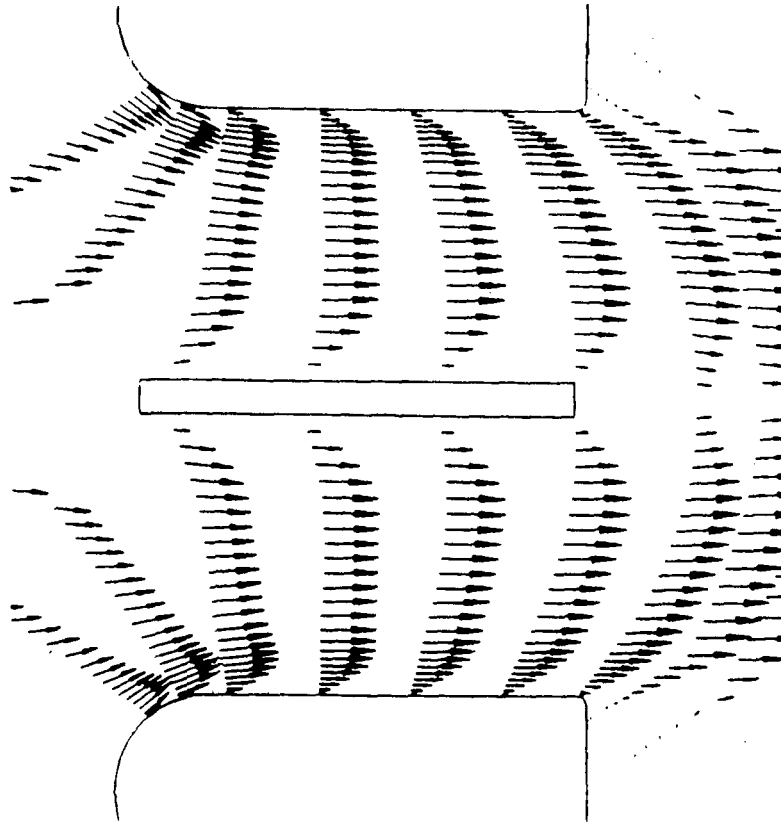of Two Struts with (Bottom) and Without Spacers Included

Fig. 10 Velocity Vectors Along Selected Nodal Lines in Region Between Two Struts Showing Effect of Spacer Simulation Midway Between Them

Periodic boundary conditions are applied at the outer lateral boundaries of each zone to simulate the effect of a row of struts, or struts alternating with posts. The results in Figure 8 and 9 are seen to exhibit the expected periodic nature, with a period length of four strut widths.

Velocity vectors in the region immediately behind the strut, for the case without posts, are shown in Fig. 11. Two symmetric recirculation regions have developed, one on either side of the strut centerline. The length of the recirculation region is approximately two and a half strut widths.

The calculations discussed so far have been for zero angle of incidence. In addition to this, single block computations around a strut were performed with a 10-deg angle of attack. Results to date indicate that the flow is unsteady; this can be seen in Fig. 12, which shows the velocity contours at non-dimensional time step intervals of 1.0. Results at a Reynolds number of 50 did not display this unsteady appearance.

3.1.2 Turbulent

Single block turbulent computations (Re = 1.9×10^6) around a two-dimensional strut were performed at zero and 10-deg angle of incidence. A Baldwin-Lomax turbulence model was used to parameterize the turbulent shear stresses. Periodic boundary conditions were applied at the lateral boundaries. The grids used in the laminar computations discussed above were modified to obtain a finer resolution near the strut surface. The average value of y^+ at the first line of nodes above the strut was approximately ten. A more refined grid would undoubtedly have provided better resolution of the near-surface flow field. However, as mentioned previously, the main purpose of the two-dimensional computations was to experiment with the implementation of various aspects of the numerical procedure as a first step toward the complete three-dimensional flowfield simulation. As such, a value of $y^+ = 10$ is considered adequate for present purposes.
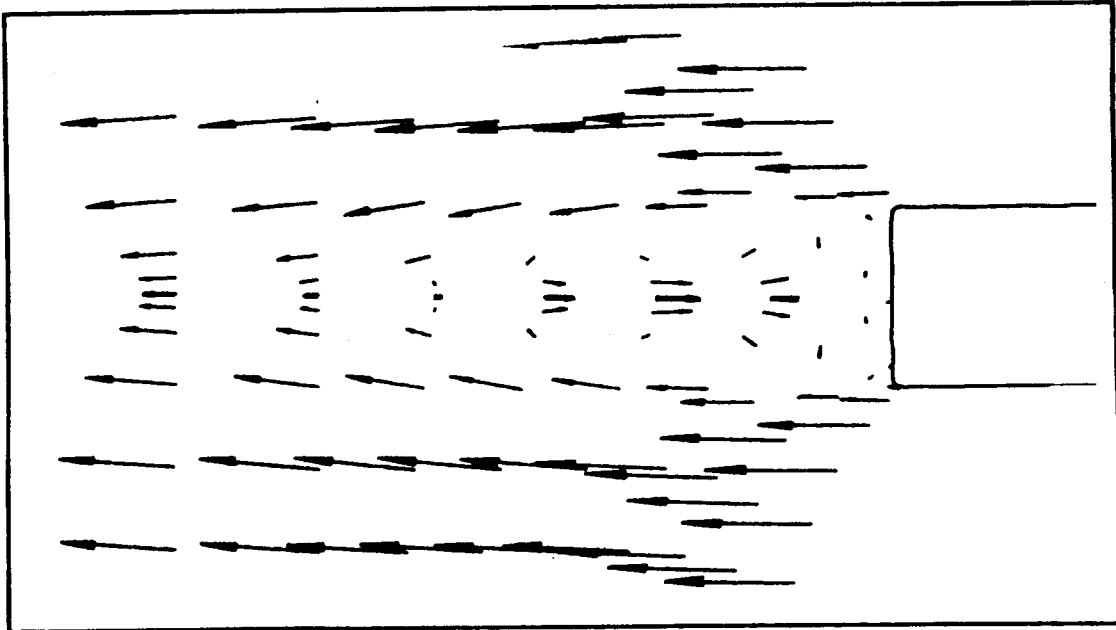
Fig. 11 Velocity Vectors Behind Strut for Two-Dimensional
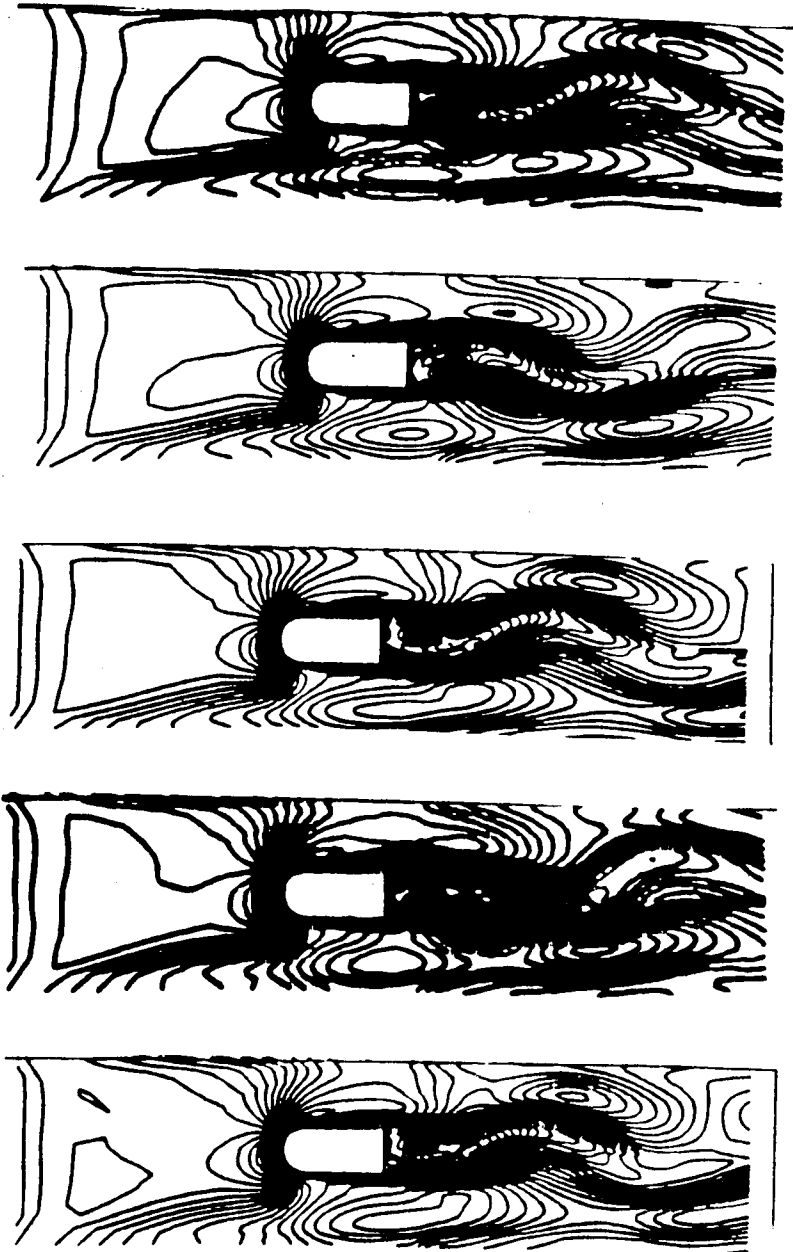Laminar Calculation Showing Recirculation Region

Fig. 12   Velocity Contours at Time Step of 1.0 for Two–Dimensional
          Laminar Flow at 10–deg Angle of Attack

24

Figure 13 shows the velocity contours around a strut for zero and 10-deg angle-of-attack. Velocity vectors in the near wake region for each of these cases is presented in Fig. 14. The size of the recirculation region is con- siderably smaller than for the laminar case (Fig. 11). As compared with the laminar 10-deg angle-of-attack results, the turbulent 10-deg angle-of- attack results did not show any noticeable unsteadiness in the velocity contours.

3.2 THREE-DIMENSIONAL COMPUTATIONS

This section presents results for flow around a strut in an annulus, a strut inside a turnaround duct, and a wing mounted on a flat plate. The type of flow which occurs when an obstruction is placed within an approaching boundary layer is typically referred to as wing-body junction or corner flow. Perhaps its most dominant feature is a horseshoe vortex system that is caused by steep adverse pressure gradients set up at the junction of the obstruction (in this case the strut) and the body (i.e., the annulus or turnaround duct). As a result of these pressure gradients, the vorticity in the oncoming boundary layer wraps around the obstruction in a characteristic horseshoe shape, with each leg having vorticity of opposite rotational sense.

3.2.1 Strut in an Annulus

Laminar (Re = 500) and turbulent (Re = 1.9 x 106) calculations were performed to simulate the flow around a strut in an annulus, as shown in Fig. 6a. The modified Baldwin-Lomax model was used in the turbulent calculations.

Both the laminar and turbulent results displayed essentially the same flowfield features, including the presence of the characteristic horseshoe vortex system. Because of this, and because of their greater relevance to the HGM flow field, only the turbulent computations will be discussed here. The average value of y^+ on the first plane of grid points off the strut was approximately seven. On the lower and upper annulus surfaces the average value was about 1.5.
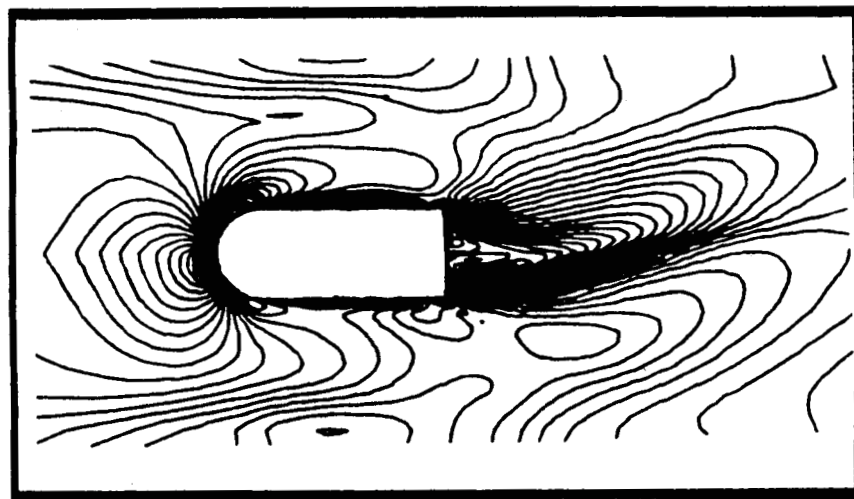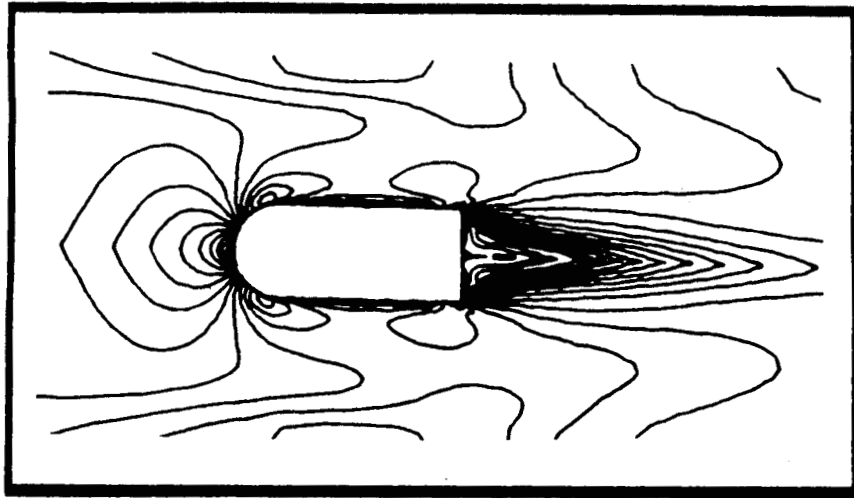
LOCKHEED-HUNTSVILLE ENGINEERING CENTER

Fig. 13 Velocity Contours for Two-Dimensional Turbulent Flow at Zero (Top) and 10-deg Angle of Attack
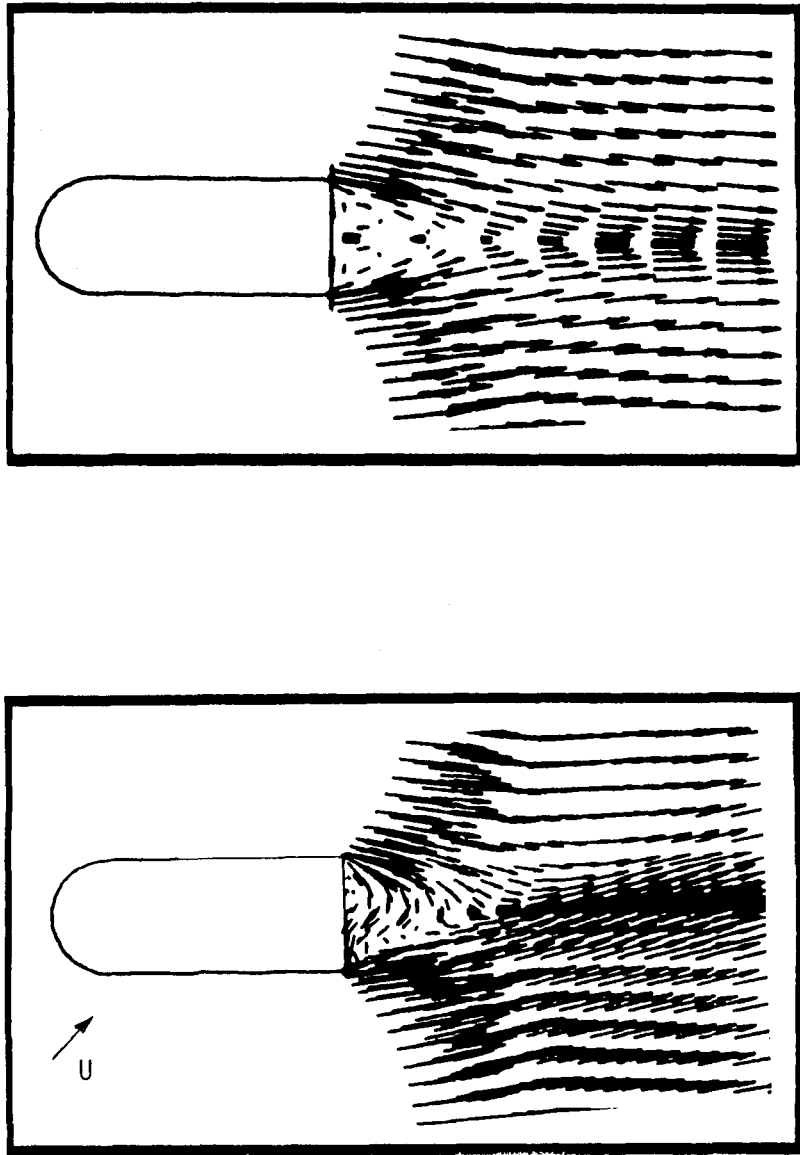
26

Fig. 14 Velocity Vectors Behind Strut for Two–Dimensional Turbulent
Flow at Zero (Top) and 10–deg Angle of Attack

Figure 15 shows simulated oil flow lines on the lower and upper annulus surfaces, respectively. The oil flow lines are seen to diverge and wrap around the strut in the characteristic horseshoe shape. The size and shape of the horseshoe vortex system for the lower annulus surface is about the same as that of the upper surface.

Figure 16 presents particle traces for particles released at various points ahead of the strut. Two spiraling vortex systems are observed behind the strut; one system is associated with the lower annulus surface, and the second with the upper surface. The difference in size between the two systems is due to the asymmetry of the annulus geometry. A similar phenomenon has been found for laminar flow of a cylinder on a flat plate (Ref. 10).

Velocity vectors in the near-wake region of the strut midway between the annulus walls are presented in Fig. 17. The size of the recirculation region is approximately the same as for the turbulent flow around a two-dimensional strut, discussed earlier in Section 3.1.

3.2.2 Strut in a Turnaround Duct

Turbulent, multiple-zone calculations were performed for the flow around a strut in a turnaround duct configuration, the geometry of which is shown in Fig. 6b. Both the modified Baldwin-Lomax and mixing length turbulence models were applied to this case. As discussed previously in Section 2.5.2, the vorticity model is relatively simpler than the modified Baldwin-Lomax approach, and allows for a smooth variation of the turbulent length scale and eddy viscosity. Due to these advantages, most of the computational effort was focused on the vorticity model. Further investigation of the differences between these models and their effect on the flowfield solution would be worthwhile.
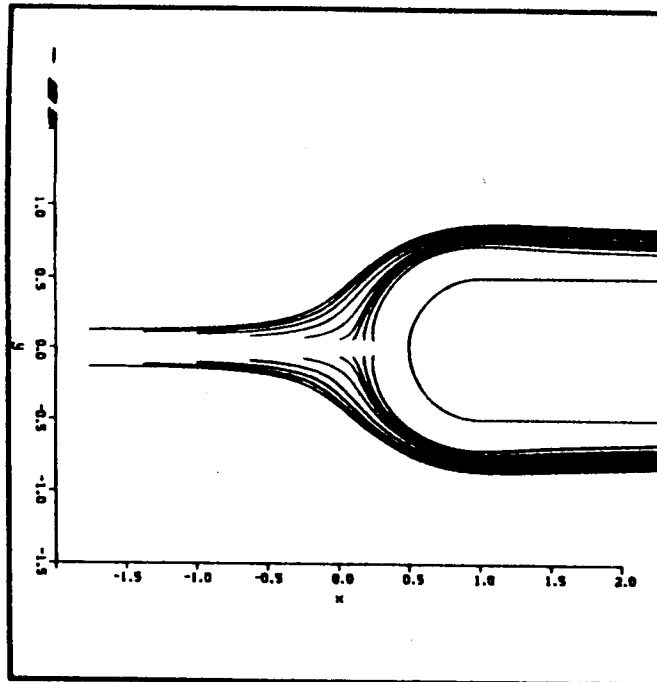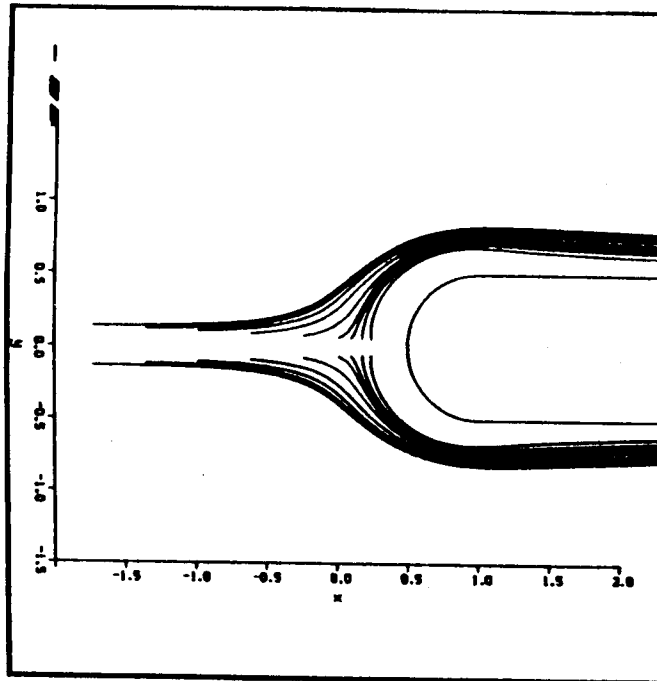
28

Fig. 15   Simulated Oil Flow Streamlines at Upper (Top)
and Lower Annulus Surfaces

29

LOCKHEED-HUNTSVILLE ENGINEERING CENTER
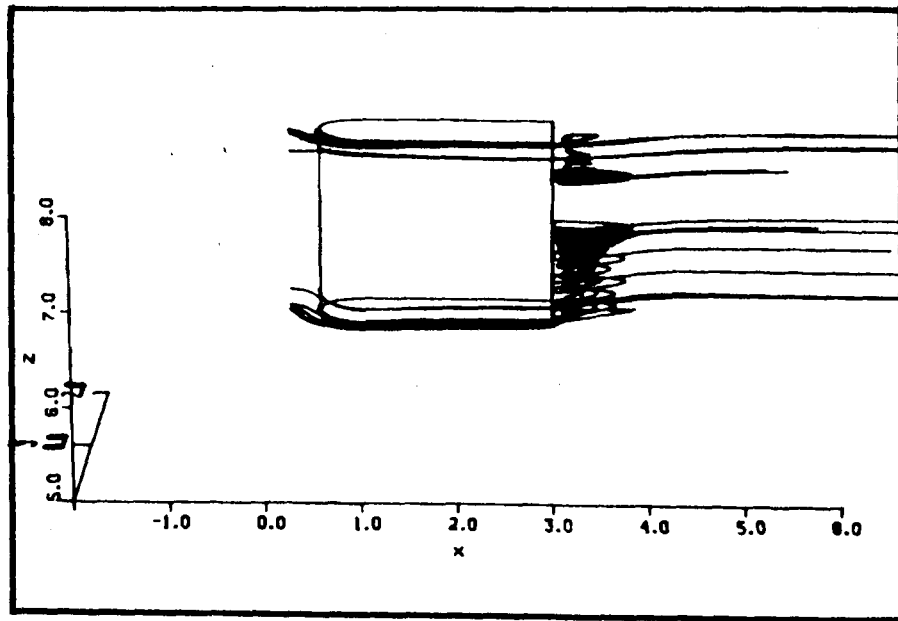
Fig. 16   Particle Traces
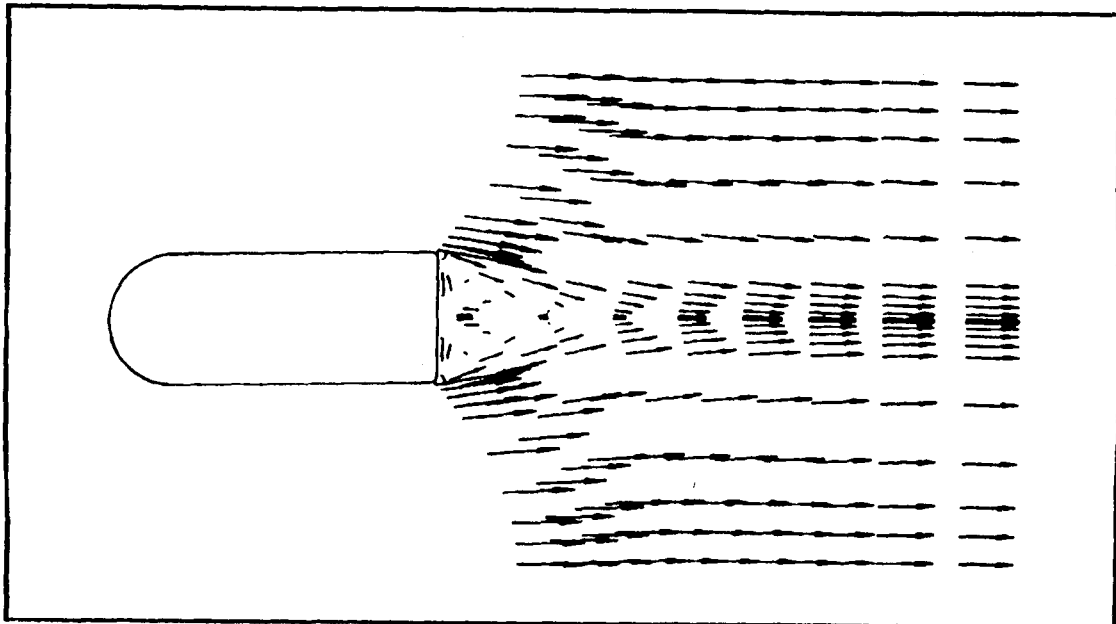
Fig. 17   Velocity Vectors Behind Strut Midway Between
Lower and Upper Annulus Surfaces

30

LOCKHEED-HUNTSVILLE ENGINEERING CENTER

Figure 18 shows the velocity contours at the central vertical plane, passing through the centerline of the strut. The inside bend of the turn-around duct is the region of highest velocity. Another region of high velocity is near the outer wall ahead of the strut. The velocity contours are seen to be smooth and continuous across the zonal boundary interface, thus giving confidence in the applicability and implementation of the multiple-zone method. A region of separation exists behind the strut, as shown in Fig. 19, which presents velocity vectors for the near wake region.

Figure 20 shows the pressure distribution on the strut and inner turn-around duct wall. The region of highest pressure is located on the strut leading edge. As the flow accelerates around the strut there is a resulting drop in pressure, followed by a pressure rise toward the trailing strut edge.

The pressure distributions along the inner and outer walls from the inlet to the leading edge of the strut is shown in Fig. 21. There is a strong adverse pressure gradient along the inner wall near the 180-deg bend. Along the outer wall, there is a favorable pressure gradient. These trends, as well as the magnitudes of the pressure coefficient, agree with other results (Ref. 4) for flow in an axisymmetric 180-deg turn around duct. A region of adverse pressure gradient ahead of the strut is observed on both the inner and outer walls, and is responsible for the skewing of the vorticity in the oncoming boundary layer.

Figure 22 shows the simulated oilflow streamlines at the inner and outer strut/turnaround duct wall juncture regions between the strut and the inner and outer turnaround duct walls. The horseshoe vortex system at the outer wall is smaller than that at the inner wall. This discrepancy is likely due to the differences in the incoming velocity profile associated with the inner and outer walls. The flow approaching the strut on the outer wall is relatively higher than at the inner wall, and will thus have more energy, and be better able to withstand the adverse pressure gradients ahead of the strut. As a result, there will be relatively less separation, and a correspondingly smaller horseshoe vortex system.
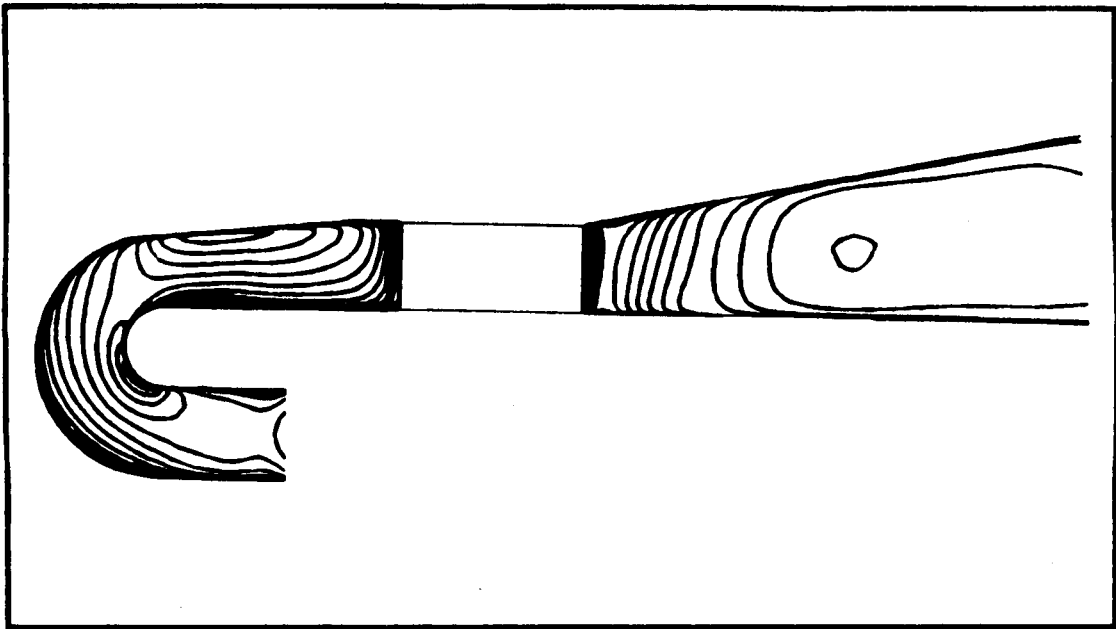
31

Fig. 18   Velocity Magnitude Contours in Vertical Plane
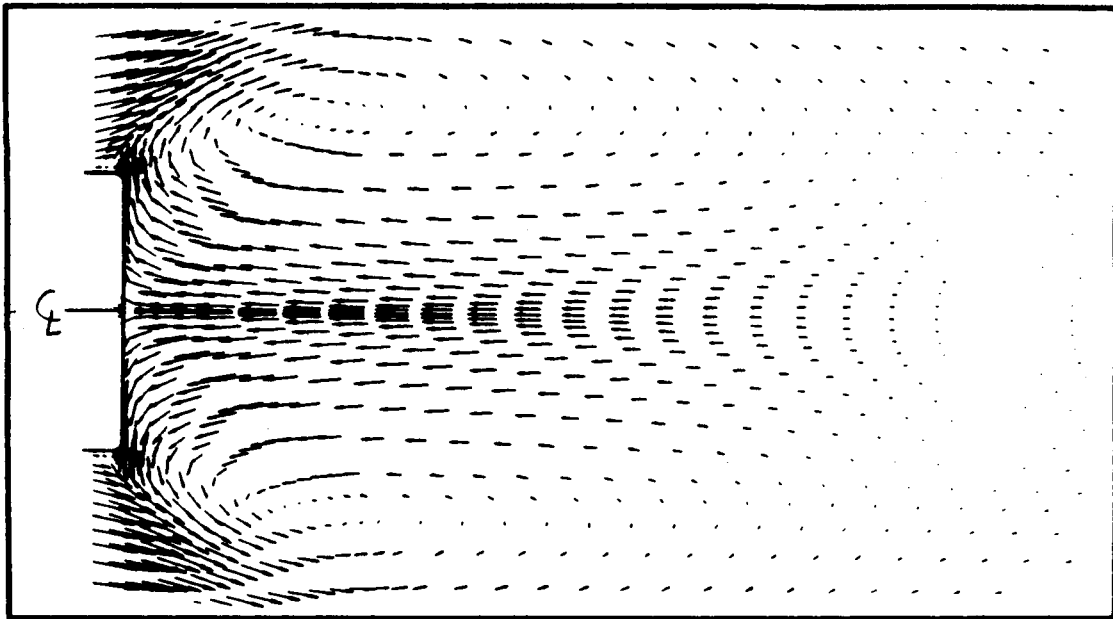Passing Through Strut Centerline

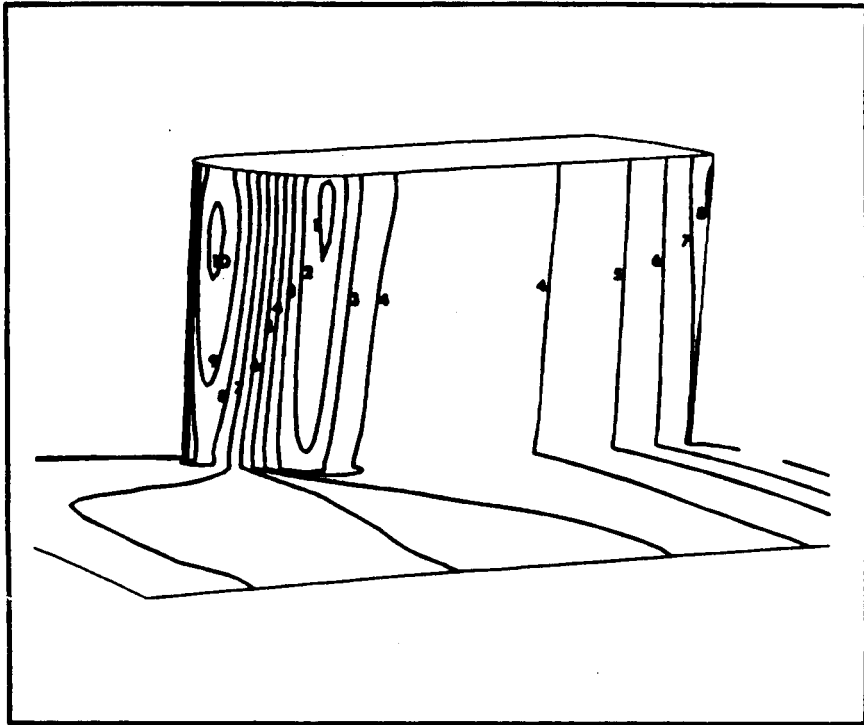Fig. 19   Velocity Vectors Behind Strut

Fig. 20   Pressure Contours on Strut and Inner
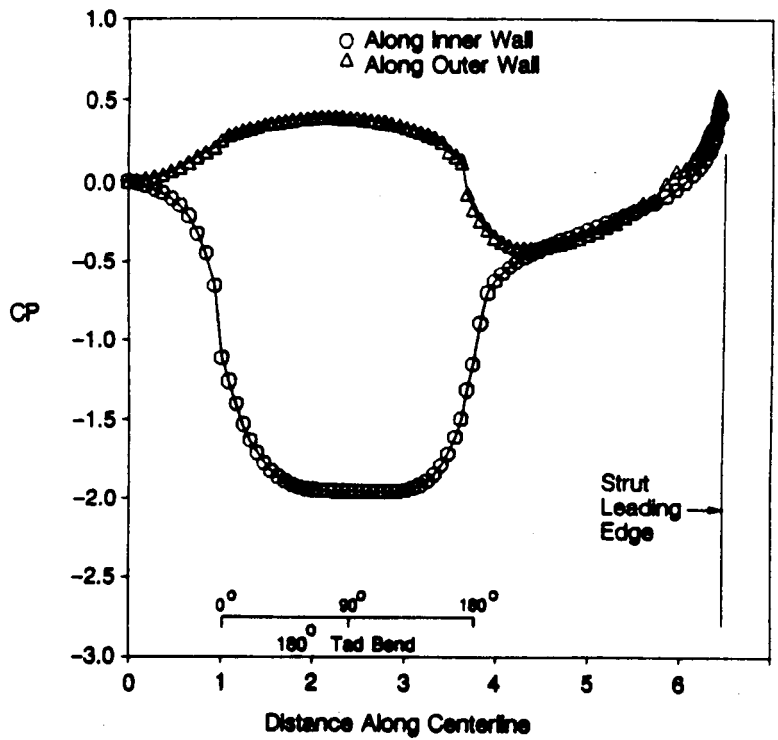Turnaround Duct Wall

Fig. 21   Pressure Distribution on Inner and Outer Turnaround Duct
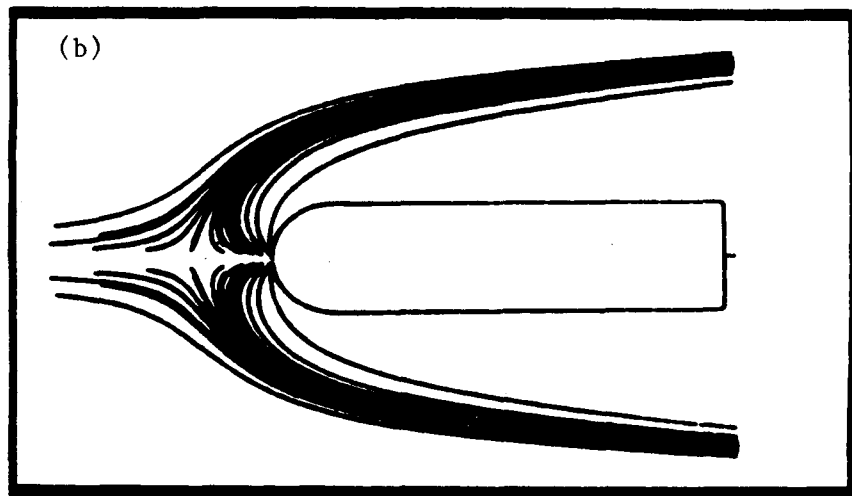Walls in Vertical Plane Passing Through Strut Centerline

33
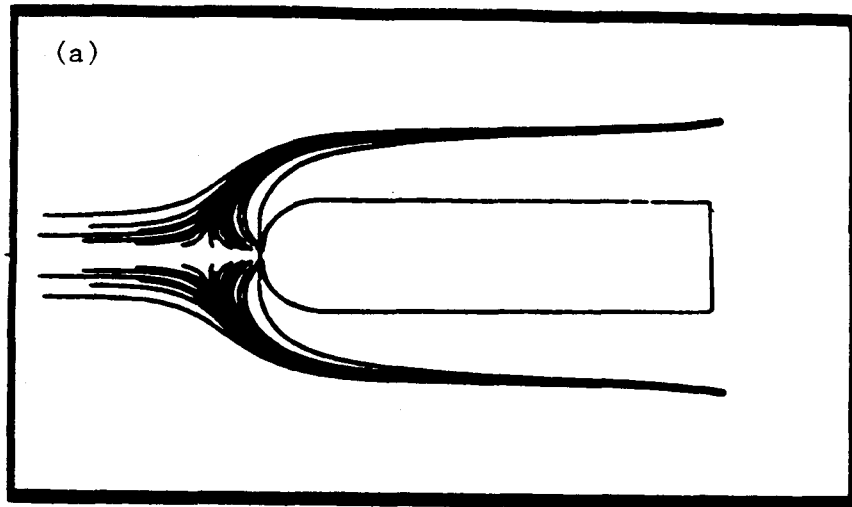
Fig. 22   Oil Flow Streamlines at Juncture Region Between Strut
and Outer Turnaround Duct Wall (a) and Lower Turnaround
Duct Wall (b)

34

Figure 23 shows the mass-weighted average total pressure distribution through the system. A slight total pressure rise is observed in the 180-deg bend of the turnaround duct. The cause of this unphysical behavior is not known, and warrants further investigation. From this figure it is seen that most of the total pressure loss occurs in the region aft of the strut, where there is considerable flow separation, as shown in Fig. 19.

Fig. 23   Total Pressure Loss

LOCKHEED-HUNTSVILLE ENGINEERING CENTER

3.2.3 Wing on a Flat Plate

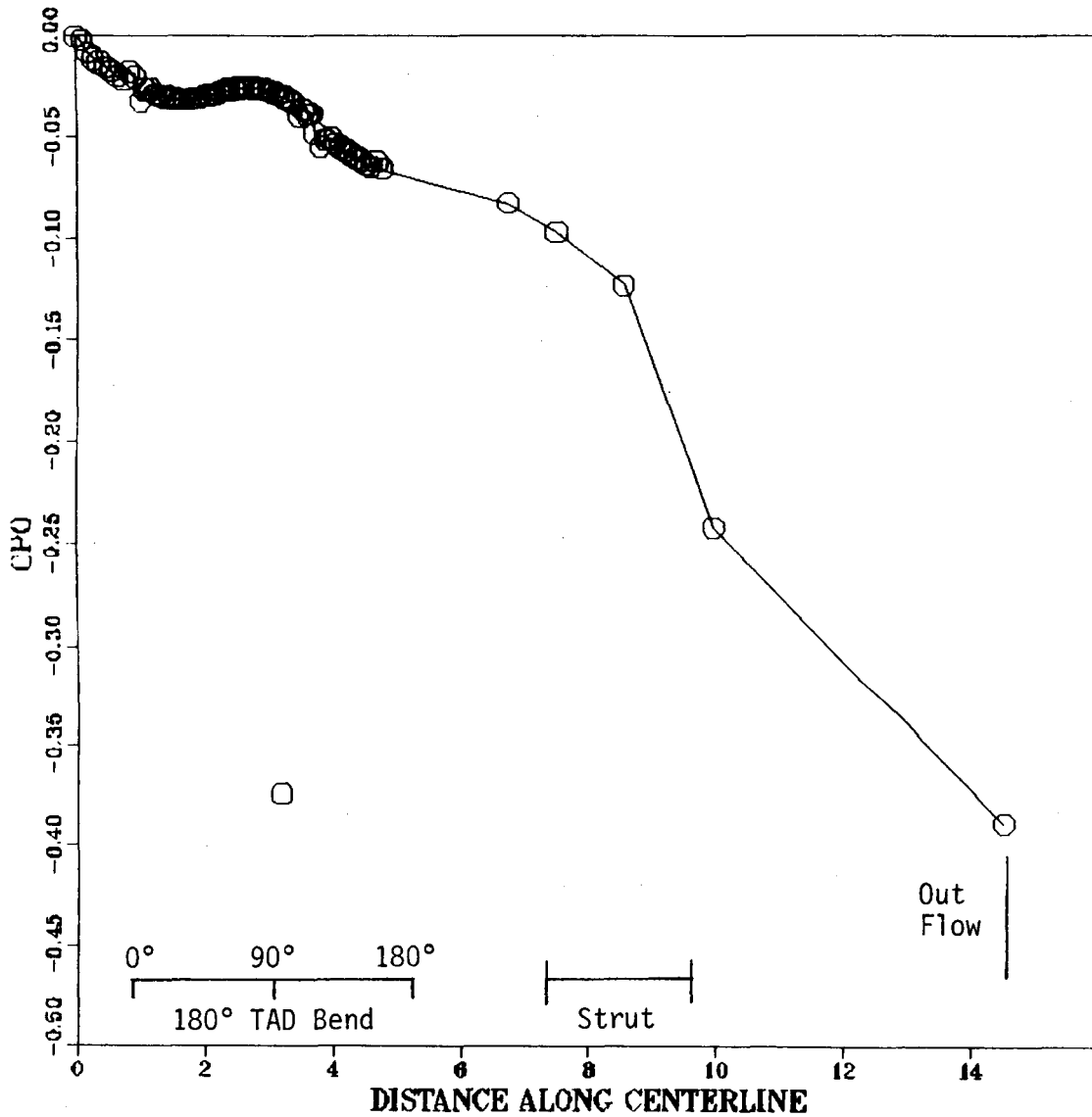In order to study the applicability of the proposed methodology, calcu-- lations were performed for external flow around a wing mounted on a flat plate, and results compared against experimental wind tunnel data of Dickinson (Ref. 11). The mixing length turbulence model was used to achieve closure.

The flowfield geometry shown in Fig. 6c consists of a wing mounted on a flat plate. The coordinate system is oriented so that the origin is at the leading edge of the wing on the flat plate, with x in the streamwise direction, y along the flat plate, and z normal to the flat plate.

Figure 24 shows the observed and predicted incoming velocity profile 3/4 of a chord length upstream of the leading edge of the wing (x/c = -.75) at the plane of symmetry (y = 0.0). The experimental and computed values agree quite well, both in magnitude and slope.

Comparisons of pressure on the flat plate along the line of symmetry (y = 0.0) and y/c = .147 are shown in Fig. 25. The observed values of pressure for the symmetry plane (y = 0.0) exhibit the steep adverse pressure gradient responsible for the skewing of the vorticity in the incoming boundary layer. The computed pressure distribution for the symmetry plane shows the same trend as the observed values, although the magnitudes are slightly overpredicted. For y/c = .147 the agreement is better. The flow accelerates around the appendage, with a resulting drop of pressure, reaching a pressure minimum near the maximum appendage thickness. This is followed by a region of pressure recovery as the appendage geometry thins. The slight rise in pressure near the trailing edge is due to the stagnation point located there.

Figure 26a shows the experimental oil flow lines on the flat plate as recorded by Dickinson (Ref. 11); the simulated oil-flow lines are shown for comparison in Fig. 26b. As the oil streaks approach the wing they are seen to diverge and wrap around the appendage in the characteristic horseshoe shape. The experimental and simulated oil flow lines are seen to be in very good
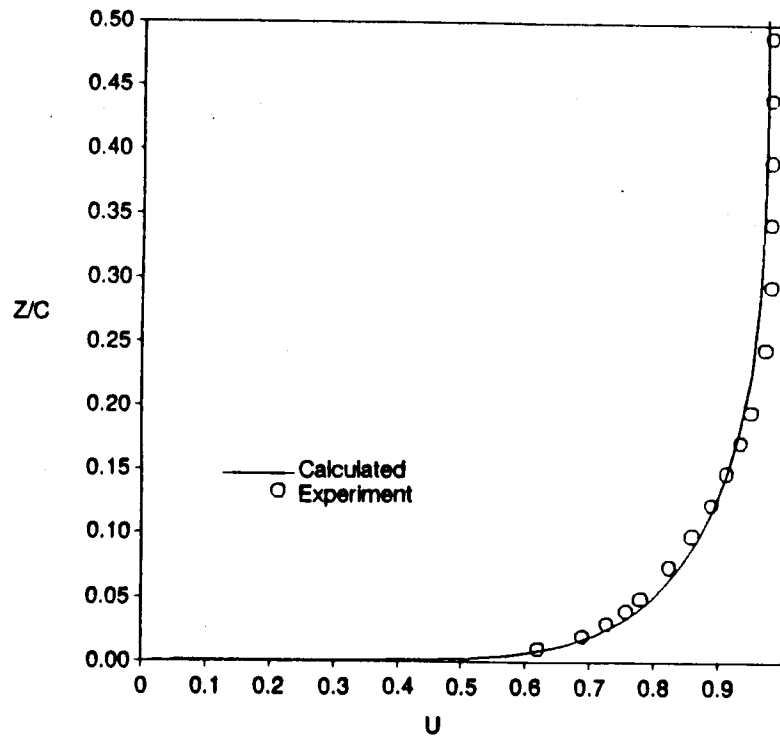
Fig. 24   Incoming Velocity Profile 3/4 Chord Length Ahead
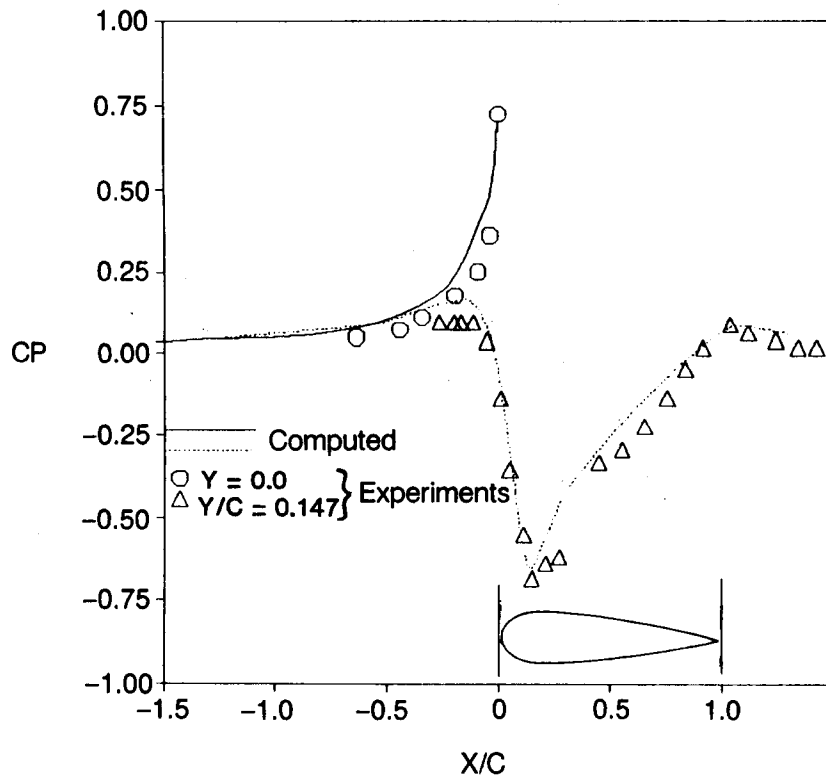of Wing (x/c = –0.75) at Symmetry Plane (y = 0.0)

Fig. 25   Pressure on Flat Plate Along y = Constant Lines:

agreement, both in overall shape and size of the root horseshoe vortex sys-
tem. The leading edge separation point is located about 0.1 chord lengths
upstream of the wing leading edge in both experiments and computations. The
primary separation lines springing from the separation point wrap around the
appendage, and then trail off downstream in a "V" type pattern. This pattern
is observed in both the observed and calculated streamlines. The particle
paths in the plane of symmetry (Fig. 27) show the separation of the flow
ahead of the wing.

Figure 28 shows velocity magnitude contours for the x = constant plane
located 3/4 chord lengths downstream of the wing leading edge (x/c = 0.75).
Both experimental and calculated results show a thin boundary layer develop-
ing on the wing. The "kinks" in the contours near the wing, visible in both
figures, are the result of the horseshoe vortex system taking high velocity
fluid away from the wall and transporting it downward into the wing-flat
plate corner region (Ref. 11).

The velocity distribution away from the wing (in the y direction) is
presented in Fig. 29, which shows streamwise velocity profiles at x/c = .75
for z/c = 0.0098, 0.0196, 0.049, and 0.1225. Again, the agreement between
observed and predicted values is generally favorable. The region of high
velocity near the wing-flat plate juncture is due to the horseshoe vortex
system.
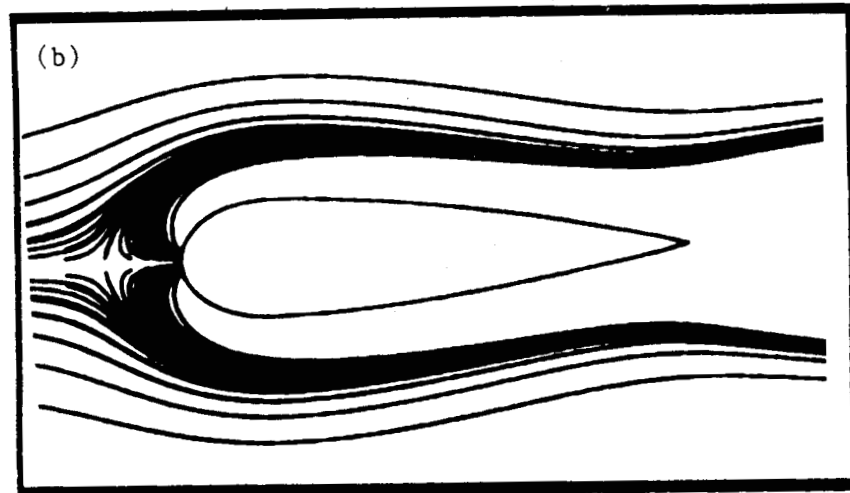
Fig. 26 Oil Flow Lines on Flat Plate
(a) Experimental (Ref. 11)
(b) Computed

39

Fig. 27 Particle Paths in Symmetry Plane (y = 0.0) Ahead of Wing

40

Fig. 28 Velocity Magnitude Contours in x = Constant Plane for x/c = 0.75:
(a) Experimental (Ref. 11)
(b) Computed

41

Fig. 29 Streamwise Velocity Profiles Away from Wing (in y Direction)
at x/c = 0.75 for z/c = Constant:
(a) z/c = 0.0098; (b) z/c = 0.0196
(c) z/c = 0.049;   (d) z/c = 0.1225

LOCKHEED–HUNTSVILLE ENGINEERING CENTER

4. CONCLUDING REMARKS
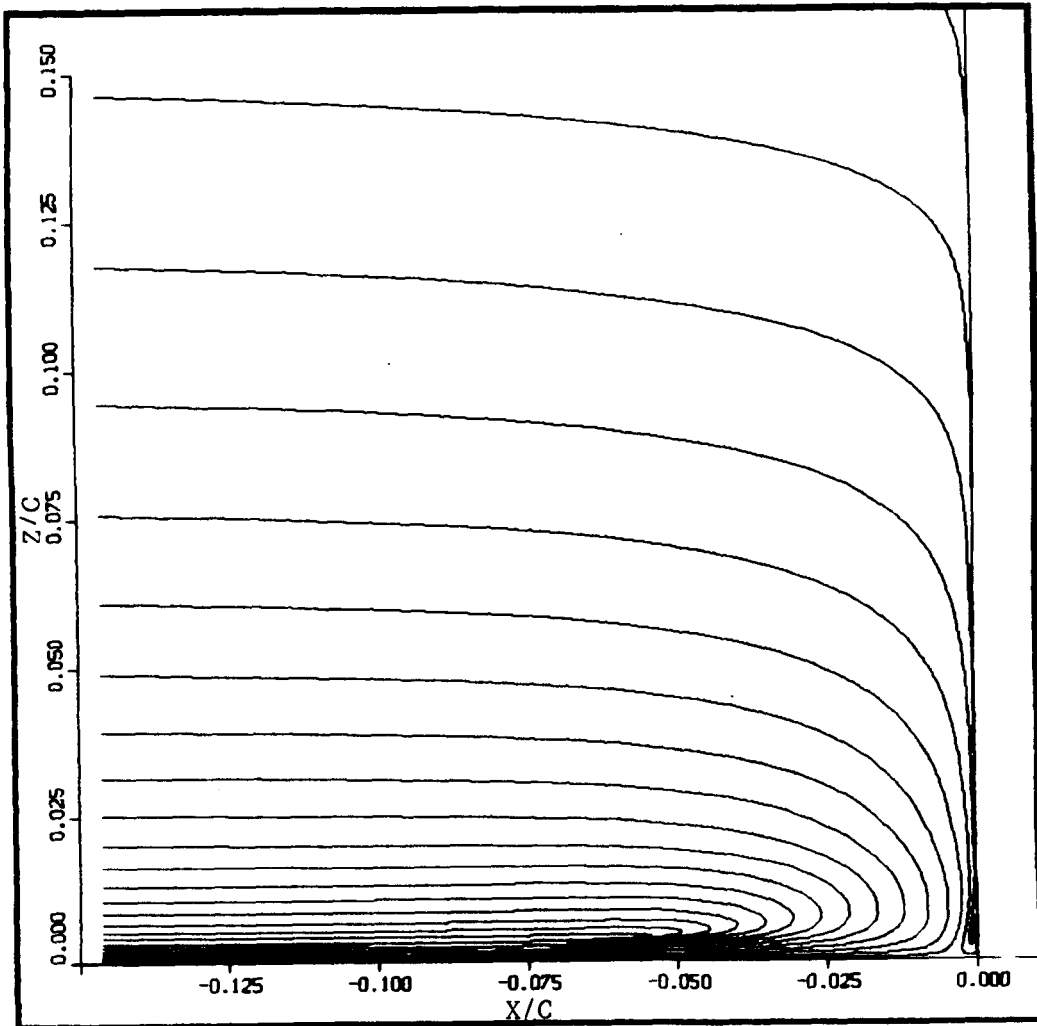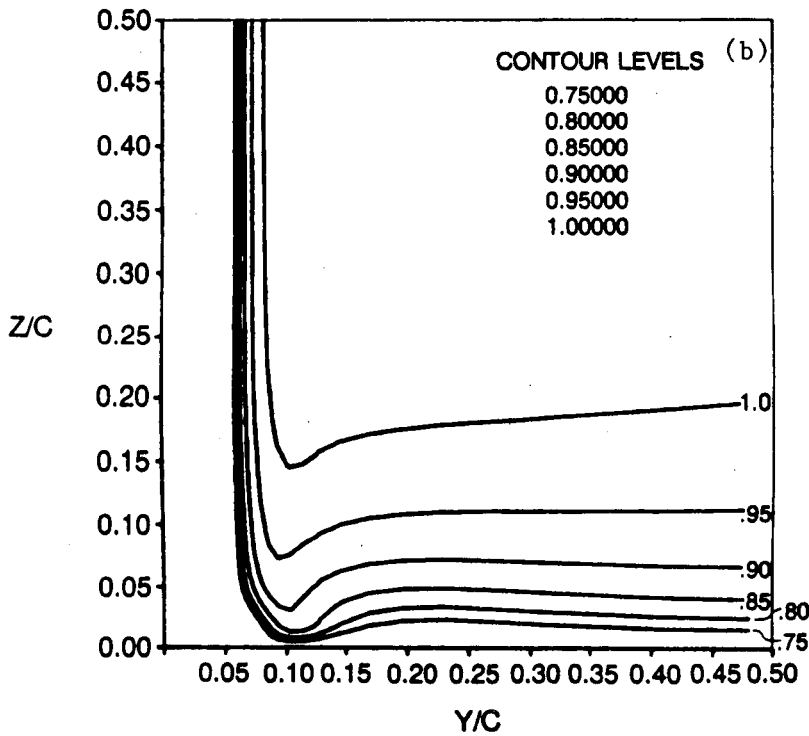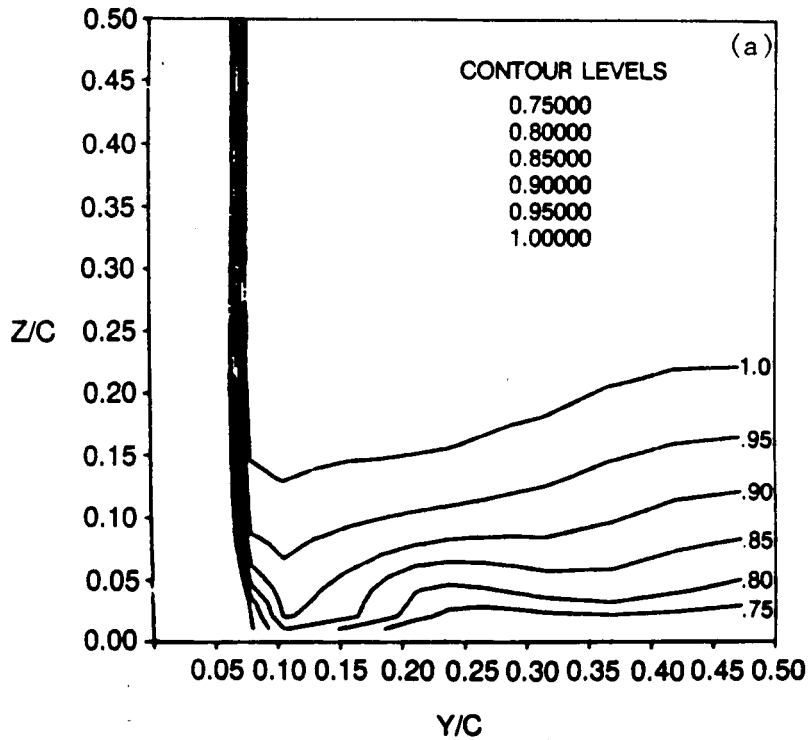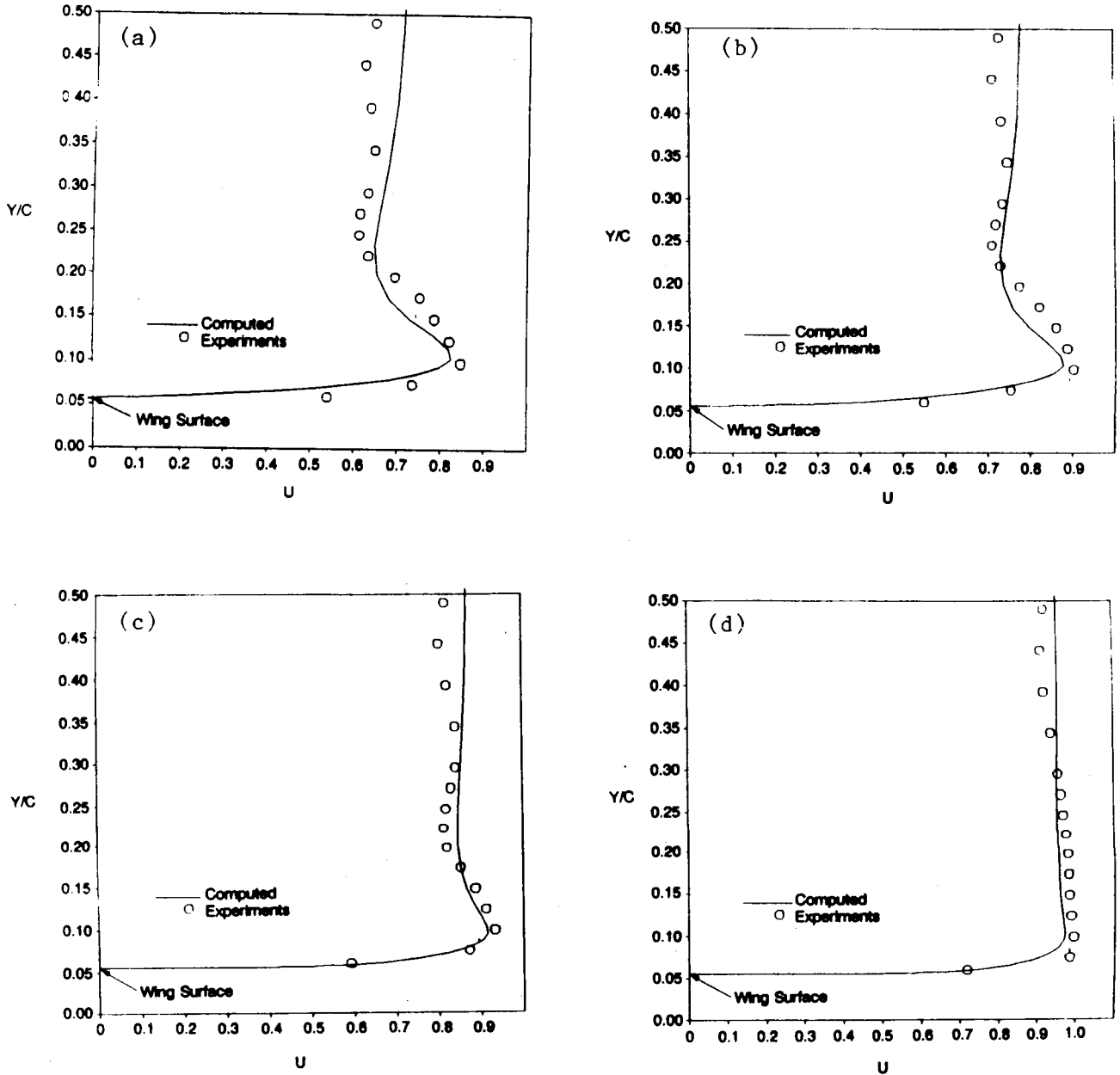
This report has presented a numerical study, using the INS3D flow solver, of laminar and turbulent flow around a two-dimensional strut, three-dimensional internal flow around a strut in an annulus and a strut in a turnaround duct, and external flow around a wing mounted on a flat plate. A multiblock proce-dure was used to calculate two-dimensional laminar flow around two struts in parallel, with each strut represented by one computational block. Single block calculations were performed for turbulent flow around a two-dimensional strut, using a Baldwin-Lomax turbulence model to parameterize the turbulent shear stresses.

A modified Baldwin-Lomax model was applied to the case of a three-dimensional strut in an annulus. The results displayed the essential features of wing-body flows, including the presence of a horseshoe vortex system at the junction of the strut and the lower annulus surface. A similar system was observed at the upper annulus surface.

A three-dimensional two block turbulent calculation of the flow in the turnaround duct (TAD) and strut/fuel bowl juncture region was also completed. The grid for the TAD comprised one computational zone and was joined, using a two-plane overlap multiblock technique, to the strut/bowl grid, which was the second computational zone. Only one strut was considered with periodic boun-dary conditions to simulate a row of struts. The fuel bowl was simulated by a streamwise variation of the cross-sectional area aft of the strut. Turbulence closure was achieved using both a modified Baldwin-Lomax model and a vorticity approach. This latter model is considered more appropriate for internal strut flows, since it allows a smooth variation of both mixing length and eddy viscosity throughout the flow field.

The results of the strut in a turnaround duct case displayed a smooth variation of pressure and velocity across the zonal interface, giving confidence in the two-plane overlap multiblocking technique. The size of the horseshoe vortex was smaller at the outer strut/turnaround duct junction than at the inner surface. This difference is believed due to the relatively higher inflow velocities near the outer turnaround duct wall ahead of the strut. The pressure distributions along the inner and outer walls in the 180-deg bend of the turnaround duct displayed similar behavior to earlier work (Ref. 4) using a different turbulence model. A region of adverse pressure gradient was observed on both walls ahead of the strut.

The mixing length turbulence model was applied to the case of external flow around a wing mounted on a flat plate. Comparisons against wind tunnel data (Ref. 11) revealed generally good agreement with the main flow features, including mean static pressure on the flat plate, size of the horseshoe vortex system, and velocity magnitudes 3/4 chord length downstream of the leading edge of the wing.

This study has developed the capability to perform turbulent multiblock internal flow calculations around obstructions using a simple algebraic turbulence model. The extension of this methodology to the complete HGM would greatly increase the understanding of the effect of the struts on the flowfield environment, including such phenomena as blockage, downstream wake patterns, and turning of the flow as it passes the strut into the fuel bowl and transfer ducts.

LOCKHEED-HUNTSVILLE ENGINEERING CENTER

5. REFERENCES

1. Kwak, D., J.L.C. Chang, S.P. Shanks, and S.R. Chakravarthy, "A Three-Dimensional Incompressible Navier-Stokes Flow Solver Using Primitive Variables," AIAA Journal, Vol. 24, 1986, pp. 390-396.

2. Hessenius, K.A., and M.M. Rai, "Applications of a Conservative Zonal Scheme to Transient and Geometrically Complex Problems," Computers and Fluids, Vol. 14, No. 1, 1986, pp. 43-58.

3. Walters, R.W., J.L. Thomas, and G.F. Switzer, "Aspects and Applications of Patched Grid Calculations," AIAA 86-1063, AIAA/ASME 4th Fluid Mechanics, Plasma Dynamics and Lasers Conference, Atlanta, Ga., 12-14 May 1986.

4. Chang, J.L.C., D. Kwak, S.C. Dao, and R. Rosen, "A Three-Dimensional Incompressible Flow Simulation Method and Its Application to the Space Shuttle Main Engine, Part II - Turbulent Flow," AIAA-85-1670, AIAA 23rd Aerospace Sciences Meeting, Reno, 14-17 January 1985.

5. Holst, T.L., U. Kayivak, K.L. Gundy, S.D. Thomas, J.L. Flores, and N.M. Chanderjian, "Numerical Solution of Transonic Wing Flows Using an Euler/Navier-Stokes Zonal Approach," AIAA-85-1640, AIAA 23rd Aerospace Sciences Meeting, Reno, 14-17 January 1985.

6. Baldwin, B.S., and H. Lomax, "Thin Layer Approximation and Algebraic Model for Separated Turbulent Flows," AIAA Paper 78-257, Huntsville, Ala., January 1978.

7. Mehta, U., K.C. Chang, and T. Cebeci, "A Comparison on Interactive Boundary Layer and Thin-Layer Navier-Stokes Procedures," Numerical Physical Aspects of Aerodynamic Flows III, ed. T. Cebeci, Springer-Verlag, 1986.

8. Gorski, J.J., T.R. Govindran, and B. Lakshminarayana, "Computation of Three-Dimensional Turbulent Shear Flows in Corners," AIAA Journal, Vol. 23, No. 5, 1985, pp. 685-692.

9. Buning, P.G. and J.L. Steger, "Graphics and Flow Visualization in Computational Fluid Dynamics," Proceedings of the AIAA 7th Computational Fluid Dynamics Conference, Cincinnati, 1985.

10. Kaul, U.K., D. Kwak, and C. Wagner, "A Computational Study of Saddle Point Separation and Horseshoe Vortex Systems," AIAA-85-0182, AIAA 23rd Aerospace Sciences Meeting, Reno, 14-17 January 1985.

11. Dickinson, S.C., "An Experimental Investigation of Appendage-Flat Plate Junction Flow, Volumes 1 and 2," David Taylor Naval Ship Research & Development Center, Bethesda, Md., DTNSRDC Reports 86/051 and 86/052, December 1986.